CNWRA 94-024

SINGLE FRACTURE FLOW BEHAVIOR OF APACHE LEAP TUFF UNDER NORMAL AND SHEAR LOADS

Prepared for

Nuclear Regulatory Commission
Contract NRC-02-93-005

Prepared by

Center for Nuclear Waste Regulatory Analyses
San Antonio, Texas

October 1994

SINGLE FRACTURE FLOW BEHAVIOR OF APACHE LEAP TUFF UNDER NORMAL AND SHEAR LOADS

Prepared for

Nuclear Regulatory Commission
Contract NRC-02-93-005

Prepared by

Sitakanta Mohanty
Asadul H. Chowdhury
Sui-Min (Simon) Hsiung
Mikko P. Ahola

Center for Nuclear Waste Regulatory Analyses
San Antonio, Texas

October 1994

ABSTRACT

Significant coupled thermal, mechanical, and hydrological interactions are likely to take place in the perturbed zone at the Yucca Mountain site. The overall objectives of the coupled thermal, mechanical, and hydrological laboratory experiments are to understand the key parameters affecting the mechanical-effect-dependent fracture flow and to provide a database that could be used to evaluate current capabilities for calculating such fracture flow. The coupled experiments have been organized to progress from simple to more complex experiments. This report presents the initial exploratory results of the mechanical-hydrological experiments that have been conducted at the Center for Nuclear Waste Regulatory Analyses on a single-jointed Apache Leap tuff specimen.

The activities reported herein include the modification of a direct shear test apparatus called "basic apparatus" to conduct radial flow under normal load, linear flow under normal load, and linear flow under combined normal and shear loads. The steady-state radial flow experiments show significant channelling in the fluid flow through rock fractures. The linear flow experiments indicate that the fracture permeability changes with the change of normal load on the rock joint. When the specimen is subjected to combined normal and shear loads, the fracture permeability is changed due to both the production of gouge material and the change of fracture aperture because of dilation. Based on the data collected to date, a permeability change of nearly 350 percent was observed when the specimen was subjected to a combined normal stress of 5 MPa and a shear displacement of 0.0254 m (1 in.), primarily due to the production of gouge material. However, from the limited tests conducted to date, it has not been possible to separate the fracture permeability change due to gouge material production from that due to the change of fracture aperture caused by dilation.

CONTENTS

CONTENTS (Cont'd)

FIGURES

FIGURES (Cont'd)

TABLES

ACKNOWLEDGMENTS

This report was prepared to document work performed by the Center for Nuclear Waste Regulatory Analyses (CNWRA) for the Nuclear Regulatory Commission (NRC) under Contract No. NRC-02-93-005. The activities reported here were performed on behalf of the NRC Office of Nuclear Regulatory Research, Division of Regulatory Applications. The report is an independent product of the CNWRA and does not necessarily reflect the views or regulatory position of the NRC.

The authors would like to thank P.C. Lichtner and G.I. Ofoegbu for their technical reviews and W.C. Patrick for the programmatic review of the report. The authors are greatly indebted to A.M. Pickens of Southwest Research Institute (SwRI) for his diligence in performing various laboratory tests for this study. Special appreciation goes to R.D. Manteufel for designing and conducting the radial flow experiments. The authors also thank D.D. Kana of SwRI for his continuing technical support in modifying the direct shear apparatus for conducting tests for this study. Thanks also go to E. Cantu and L. Hearon for assisting with word processing and to SwRI Publications Services for the editorial review.

QUALITY OF DATA

All CNWRA-generated original data contained in this report meet the quality assurance requirements described in the CNWRA Quality Assurance Manual.

EXECUTIVE SUMMARY

Significant coupled thermal, mechanical, and hydrological (TMH) interactions are likely to take place in the perturbed zone at the Yucca Mountain (YM) site (Ghosh et al., 1993; 1994). The heat generated due to emplaced waste may cause water redistribution in the emplacement area due to gravity or capillary effects. The extent of this redistribution depends, among others, on the amount of heat generated from the emplaced waste. Various conceptual models (Buscheck and Nitao, 1993; 1994) have indicated that, at YM, fractures may act as major conduits for condensate flow toward the heat source (waste packages) since the matrix permeability of the Topopah Spring unit TSw2 is so small that the matrix flow in the near field is of little concern to repository performance. The amount of condensate flow may be enhanced by infiltration of rainfall. In this condition, the fracture flow tends to persist for a long distance before the condensate is revaporized or imbibed by rock matrix. Therefore, it appears that the extent of dry-out zone, the amount of condensate available above the emplacement areas, and the hydrological properties of fractures will determine the saturation conditions around the repository.

The hydrological properties of fractures may not remain constant throughout the life of the waste package and repository because of the deformation of the fractures in the perturbed zone. Due to construction activities, the state of stress around the repository may change, resulting in mechanical deformation of the rock mass. Most of the rock mass deformation will arise from normal and shear displacements on fractures (Kana et al., 1991; Hsiung et al., 1992). Fracture normal and shear deformations will affect fluid flow and solute transport in the rock mass through changes in fracture aperture. Rock thermal expansion may also cause dilation, closure, and shear failure of fractures, thus leading to changes in hydrological properties of fractures. Dynamic ground motion due to earthquakes, nearby underground weapons testing, etc., will take place in the environment of *in situ* stresses and thermally induced phenomena in the repository. The dynamic ground motions, including the cumulative effect of repetitive seismic motions (Hsiung et al., 1992), will cause further dilation, closure, and shear of fractures. The cumulative effects of repetitive seismic loads may form preferential pathways connecting the emplacement area with the condensation zones above the emplacement area or perched water zones. These preferential pathways could increase significantly the chance for water to contact waste packages. Rock strength properties may also change with time due to rock mass deterioration. Furthermore, deterioration of the rock mass surrounding the repository may continue after permanent closure if the backfill is not sufficient to support the rock mass on the top of the drifts. These phenomena may increase the capability of fractures to conduct flow. Since pore water or vapor in the rock matrix tends to expand in volume as temperature increases, some have postulated pore pressure buildup (Althaus et al., 1994). Since the rock matrix permeability at YM is low, the buildup in pore pressure may not be relieved quickly. The possible consequences of these potential effects are not currently understood.

Consequently, the ability to characterize these effects is important in evaluating performance of waste packages. In addition to TMH interactions, the flow field may be altered by precipitation or dissolution of minerals, which will either decrease or increase the permeability of the fracture network (Lin and Daily, 1989; de Marsily, 1987). The effect of chemical reactions on the TMH processes, and vice versa, was not considered in this study, but may be considered at a later date.

To address mechanical-effect-dependent fluid flow through fractures, that is, coupled TMH interactions on fracture flow in the near field, the Center for Nuclear Waste Regulatory Analyses (CNWRA) has undertaken a program of research and development on coupled TMH processes. The study on coupled TMH processes is being conducted through: (i) participating in modeling within the international

cooperative project DECOVALEX (acronym for the DEvelopment of COupled models and their VALidation against EXperiments in nuclear waste isolation), (ii) performing coupled TMH laboratory experiments, and (iii) conducting model validation and code verification work to develop compliance determination method codes. The second activity is the subject of this report.

The overall objectives of the coupled TMH laboratory experiments are to understand the key parameters affecting the mechanical-effect-dependent fracture flow and to provide a database that can be used to evaluate current capabilities for calculating such fracture flow. The coupled experiments were organized to progress from the simple to the more complex experiments. This report presents the results of the mechanical–hydrological experiments that were conducted at the CNWRA on a single-jointed Apache Leap tuff specimen.

During this phase of work, an apparatus was developed by modifying a direct-shear test apparatus (Hsiung et al., 1994) to measure change in fracture permeability under normal and shear loads. Initially, a radial flow configuration was adopted for conducting flow studies. Fluid was injected through a vertical hole on the top block. The hole extended all the way to the fracture plane of a rock joint, with the single fracture approximately aligning in the horizontal direction. Steady-state flow experiments were conducted by using three nonreacting fluids with different viscosities. These fluids were air, water, and water with a glycerol additive. Significant channeling in the fluid flow was observed. The channeling was so severe that water did not exit from one of the four sides of the rock joint. From the other three sides of the rock joint, water or water with glycerol additive came out in the proportion of 74.5, 18.4, and 7.1 percent.

To measure the flow properties of the whole fracture plane, the flow configuration was changed from radial to linear. This change in configuration required substantial modification to the experimental apparatus. A fluid-sealing mechanism was developed that is specific to this apparatus. The sealing design complexities resulted from the unequal sizes of the top and bottom blocks of the rock joint. Adding to the design difficulties was the requirement that the seal not break during shear displacement of the top block with respect to the bottom block. Such a seal mechanism was successfully implemented. Linear fluid flow experiments were conducted using air and water separately as flowing fluids.

An increase in normal stress to 8 MPa caused nearly a 35-percent change in fracture permeability. Forward and reverse normal loading showed a definite hysteresis in fracture permeability. A similar trend was observed with the mechanical aperture measurements. As expected, the fracture permeability showed a nonlinear trend with the imposed normal load.

Based on the data collected so far, a permeability change of nearly 350 percent was observed when the specimen was subjected to a combined production of gouge material and joint dilation under shear displacement. However, from the limited tests conducted to date, it was not possible to separate the permeability change due to gouge material production from that due to dilation.

The apparatus developed was capable of measuring the effect of rock-joint shear displacement of up to 0.0254 m (1 in.) on permeability, though theoretically, a displacement of up to 0.0508 m (2 in.) can be studied. Based on the test results, it appeared that the effect of shearing can be much more significant than that demonstrated in the past. However, it must be noted that the level of joint–surface damage may be a function of surface characteristics in addition to the rock mass material properties. In this regard, this experiment used Apache Leap tuff whose characteristics are similar to the welded tuff that occurs at YM. However, more tests using rocks with different material properties, and more Apache Leap

specimens, must be conducted before the results can be considered conclusive. Shear load experiments were much more difficult to perform compared to the normal load experiments, because of the extreme conditions to which the fluid sealing mechanism was subjected. These extreme conditions were complicated by the fact that shear testing is a destructive method of testing. It was evident that damage to the rough surface produced a significant amount of gouge materials. Thus, it was necessary to separate the effects of joint dilation on the flow from that of gouge material on the flow.

The existing apparatus needs modification because the severity of the shearing process opened up the components of the metal box containing the rock joint specimen causing a fluid leak. Fortunately, this leak mostly occurred during the movement of the block. A panel of differential transducers representing a broad pressure range (0.25–690 kPa) also needs to be implemented in order to quantitatively gauge the change in fracture permeability due to the gouge formation. Since formation of the gouge material will force the experiments to be conducted at higher fluid pressures, the system must also be modified accordingly to withstand such high pressures.

Numerical exercises were performed to retrieve aperture data from block surface height data. The FRAC_APR code was written that searched for the perfect mate between the two blocks. While the method seems to have found the matching position, the quantitative aperture data do not seem reasonable. Further numerical studies are necessary.

1 INTRODUCTION

1.1 BACKGROUND AND OBJECTIVES

In 1987, the U.S. Congress designated Yucca Mountain (YM), located approximately 160 km northwest of Las Vegas, Nevada, for characterization as a potential repository site for high-level nuclear waste (HLW) disposal. A general description of the YM site for the proposed repository has been given in the U.S. Department of Energy (DOE) Site Characterization Plan (SCP) (U.S. Department of Energy, 1988). The area is characterized by north to northwest trending mountain ranges composed of volcanic and volcaniclastic strata that dip eastward. The strata are broken into en-echelon fault blocks. The geomechanical conditions at the site are characterized as a highly jointed rock mass with prominent vertical and subvertical faults and joints (fractures). The potential repository location is in the densely welded, devitrified part of the Topopah Spring (TSw2 unit) member of the Paintbrush tuff, which is about 350 m below the ground surface and 225 m above the water table (Klavetter and Peters, 1986). At YM, the zone above the water table contains capillary water held tightly in pores of rock matrix, estimated at about 65 percent in saturation. There may also be potential perched water zones above the repository horizon. Repository construction and emplacement of radioactive waste in this partially saturated geologic medium are expected to cause major perturbations to the system involving coupled thermal, mechanical, hydrological, and chemical (TMHC) processes. The extent of the perturbed zone depends on many factors such as the initial state of stress, method of excavation, orientation and properties of fractures, site structural geology, the magnitude and recurrence time of seismic events, and the magnitude of thermal load.

There may be significant coupled thermal, mechanical, and hydrological (TMH) interactions in the perturbed zone at the YM site (Ghosh et al., 1993; 1994). The emplaced waste generates heat that will cause the temperature of the rock mass around the emplacement areas to rise. If the temperature in the rock mass reaches the boiling point, the pore water in the rock matrix is likely to vaporize and flow away from the emplacement areas, condensing in regions where the temperatures are below boiling conditions. Thus a dryout zone will be created (Buscheck and Nitao, 1993). The condensate in the zones above the emplacement areas tends to drain back toward the emplacement areas due to gravity or capillary effect. The extent of this saturation redistribution depends on the amount of heat generated from the waste. Key questions needing to be answered in order that the performance of waste packages can be assessed reliably include: (i) whether or not the reflux of the condensate can reach the waste packages, (ii) if so, what is the rate of condensate-flow toward the waste packages and when does the flow begin, and (iii) what is the chemical content of the condensate that may contact the waste packages? It has been argued (Buscheck and Nitao, 1994) that, at YM, fracture flow may be the most likely means for condensate to flow back toward the heat source (waste packages) since the matrix permeability of the TSw2 unit is extremely small such that the matrix flow in the near field is of little concern to repository performance. In this condition, the fracture flow tends to persist for a long distance before the condensate is revaporized or imbibed by rock matrix. It would, therefore, appear that the extent of dryout zone, amount of condensate available above the emplacement areas (note that the amount may be enhanced by infiltration of rainfall), and the hydrological properties of fractures (taking into consideration the buoyant pressure of vapor flow) are the predominant factors that will determine the answers to the first two questions posed earlier in this paragraph.

The issues are complicated further by the possibility that the hydrological properties of fractures may not remain constant throughout the life of the waste packages and repository. These properties will

be perturbed in several ways. First, the construction of the repository will change the state of stress, which, in turn, will cause mechanical deformation of the rock mass. It is postulated that most of the rock-mass deformation will arise from normal and shear displacements on fractures (Kana et al., 1991; Hsiung et al., 1992). Fracture normal and shear deformations will not only have implications regarding the stability of excavations but will also affect fluid flow and solute transport in the rock mass through changes in fracture aperture. It should be noted that excavation stability is an important concern related to waste retrievability. Excessive falls of large rock blocks may affect the performance of the waste packages during the operational and containment periods.

Second, the heat generated from the emplaced waste is expected to be active over an extended period of time. This thermal load induces rock expansion. The rock expansion may also cause dilation, closure, and shear failure of fractures, leading to changes in the hydrological properties of fractures.

Third, dynamic ground motions due to earthquakes, nearby underground weapons testing, etc., will take place in the environment of *in situ* stresses and thermally induced phenomena in the repository. The dynamic ground motions, including the cumulative effect of repetitive seismic motions (Hsiung et al., 1992), will cause further dilation, closure, and shear of fractures. A typical example of that effect of earthquakes on hydrology is what happened in California during the Loma Prieta earthquake (Rojstaczer and Wolf, 1992). In the case of the Loma Prieta earthquake, it has been inferred that the increased fracture permeability allowed the water table in the mountains to drop more than 21 m while greatly increasing the flow of springs and streams in the foothills. Hydrologic changes due to earthquakes have also been observed in connection with several other earthquakes (see, for example, Ofoegbu et al., 1994). At YM, the change of fracture permeability may occur due to the ground motion from earthquakes and underground nuclear explosions at the Nevada Test Site. Recent observations (Hill et al., 1993) that a large earthquake can induce smaller earthquakes at great distances from its epicenter makes this concern much more significant than previously thought. The cumulative effects of repetitive seismic loads may form preferential pathways connecting the emplacement area with the condensation zones above the emplacement area or perched water zones, which could increase significantly the chance for water to contact waste packages.

In addition to the three causes mentioned previously that may induce changes in fracture hydrological properties, it is well recognized that rock strength properties are a function of time (or stress), that is, rock mass deteriorates as time passes. This deterioration may be a possibility for the rock mass surrounding the repository since the potential backfill for the emplacement drifts after permanent closure may not be sufficient to support the rock mass on the top of drifts to prevent such a deterioration. The rate and extent of the deterioration depend primarily on the strength properties of fractures. All these factors are likely to increase the capability of fractures to conduct flow. Furthermore, pore water or vapor in the rock matrix tends to expand as temperature increases, causing the development of excess pore pressure. Since the rock matrix permeability at YM is low, the excess pore pressure may not dissipate quickly. Laboratory data presented by Althaus et al. (1994) suggest that such pressure increase in the rock matrix may weaken the rock enough to increase the likelihood for microfracturing. The occurrence of microfracturing may cause considerable increase in the rock-mass permeability. However, it is not yet clear how such changes in rock-mass permeability may affect the performance of the proposed repository.

In addition to the coupled TMH interactions discussed previously, there is also the concern of chemical and thermomechanical coupling with the flow field. This coupling may be related to the precipitation or dissolution of minerals, which will either decrease or increase the permeability of the fracture network (Lin and Daily, 1989; de Marsily, 1987). However, the effect of chemical reactions on

the TMH processes, and vice versa, was not considered in this study. The effect of chemical reactions on TMH processes, and vice versa, will be considered at a later date, if appropriate.

To address the issue of mechanical-effect-dependent fluid flow through fractures, that is, coupled TMH interactions on fracture flow in the near field, the Center for Nuclear Waste Regulatory Analyses (CNWRA) has undertaken a program of research and developmental technical work on coupled TMH processes. This study on coupled TMH processes is being conducted through: (i) participating in the modeling within the international cooperative project DECOVALEX (acronym for the DEvelopment of COupled models and their VALidation against EXperiments in nuclear waste isolation), (ii) performing coupled TMH laboratory experiments, and (iii) conducting model validation and code verification for the development of compliance determination method codes. The first and second activities are being conducted under the Rock Mechanics research project, and the third activity is being conducted under the Repository Design, Construction, and Operations (RDCO) subtask on Investigation of Issues Related to RDCO.

The overall objectives of the coupled TMH laboratory experiments are to understand the key parameters affecting the mechanical-effect-dependent fracture flow and to provide a database that can be used to evaluate current capabilities for calculating such fracture flow. The coupled experiments have been organized to progress from the simple to the more complex experiments. In FY93, the coupled experimental program was initiated on an exploratory basis with the radial flow study of the mechanical-hydrological (MH) coupled effects on single-jointed Apache Leap tuff specimen. In subsequent years, this program will be followed by selected two-process coupled experiments, and finally, coupled TMH experimental studies. This report presents the results of the MH experiments that were conducted at the CNWRA on a single-jointed Apache Leap tuff specimen during FY93–94.

1.2 SCOPE

The scope of work for this report on coupled MH experiments on a single-jointed Apache Leap tuff specimen includes both linear and radial flow tests. However, the primary emphasis is on linear flow experiments. The MH experimental activities reported herein include:

- Development of experimental technique
- Characterization of rock joint interfaces
- Radial flow experiments under normal load
- Linear flow experiments under normal load
- Linear flow experiments under combined normal and shear loads

2 EXPERIMENTAL APPARATUS AND ROCK JOINT SPECIMENS

The coupled MH experiments have been designed to make maximum utilization of existing direct shear test apparatus, joint profile-measuring apparatus, procedures, and single-jointed Apache Leap tuff specimens from Task 2 of the Rock Mechanics (RM) research project. The direct shear test apparatus, herein called the "basic apparatus," that was designed, constructed, and used for testing of single jointed rock specimens under combined normal and direct shear loads (Kana et al.,1991; Hsiung et al.,1994), has been modified to incorporate the hydrologic aspect of the MH experiments.

2.1 DIRECT SHEAR TEST APPARATUS (BASIC APPARATUS)

In order to perform direct dynamic shear tests on single jointed rock specimens, a test apparatus with combined normal and shear loading capability was designed, fabricated, and assembled at Southwest Research Institute (SwRI) (Kana et al.,1991; Hsiung et al.,1994). The apparatus consists of vertical and horizontal servocontrolled loading actuators, reaction frames, shear box fixtures, and an instrumented jointed tuff specimen (Figure 2-1). The loading capacity for each of the three vertical actuators is 0.133 MN, while the horizontal actuator has a capacity of 0.222 MN. The horizontal actuator can be operated in either load or displacement control mode. When needed, several loading patterns, such as pseudostatic ramps, harmonic, and earthquake displacement time histories, can be generated through the use of a function generator. Each vertical actuator is equipped with a 0.111 MN capacity load cell for monitoring the applied forces. The instrumentation for monitoring the applied normal load is arranged to provide an analog output for the sum of the three load cells, as well as for the individual signals. The bottom shear box was designed to house a specimen with maximum dimensions of $0.305 \times 0.203 \times 0.102$ m. The top shear box houses a specimen with maximum dimensions of $0.203 \times 0.203 \times 0.102$ m. Both specimens are grouted in their respective specimen boxes by using cement. The bottom shear box and other fixed devices are bolted to a $1.22 \times 2.13 \times 0.15$ m thick steel base plate for rigidity. The horizontal translation of the top shear box along the direction of shearing is guided through three rollers between the top shear box and normal load frame. It is also guided through side rollers as shown in later figures. Thus, the normal load frame and the side rollers prevent rotation of the vertical actuators (and, therefore, also the top specimen block) about a vertical axis perpendicular to the direction of shearing.

2.1.1 Normal Load System

Normal compression is applied to the specimen by three vertical actuators set at 120 degrees about the specimen's vertical centerline. These actuators act through individual load cells whose output is summed and used as the control signal. Thus, the total normal load is controlled at a preselected static or slowly ramped value. This total resultant load is ultimately applied to the specimen via the normal load frame that acts on the three normal load rollers (see top view of Figure 2-1) and thereby on the upper specimen box. The line of action for this normal load is through the null position of the upper specimen box. Thus, the normal load frame is constrained to three degrees of freedom: (i) vertical translation, (ii) rotation about the horizontal axis in line with the shear, and (iii) rotation about the horizontal axis transverse to the shear. These constraints are assured by two double flexures that connect the normal load frame to a fixed reaction brace, and by the two side roller assemblies, which act on the upper specimen box. Thus, the upper specimen block is constrained to these same degrees of freedom, plus a fourth translation in the direction of shear.

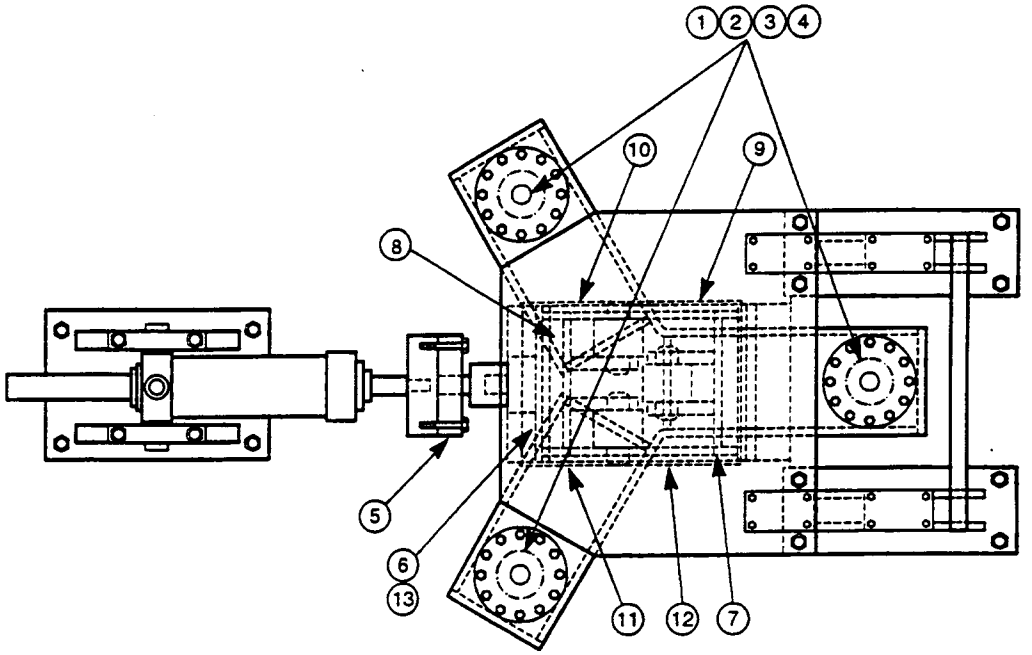

TOP VIEW

1. Vertical Load Cell No. 1
2. Vertical Load Cell No. 2
3. Vertical Load Cell No. 3
4. Analog Summation of Total Vertical Normal Load
5. Horizontal Load Cell
*6. Horizontal Displacement of Top block Relative to Bottom Block – LVDT1
8. Horizontal Displacement of Top Block Relative to Bottom Block – LVDT3
*9. Vertical Relative Displacement Proximeter No. 4
*10. Vertical Relative Displacement Proximeter No. 5
*11. Vertical Relative Displacement Proximeter No. 6
*12. Vertical Relative Displacement Proximeter No. 7
13. Horizontal Acceleration at Near Left of Upper Specimen Block
* see Figure 2-4 for exact location

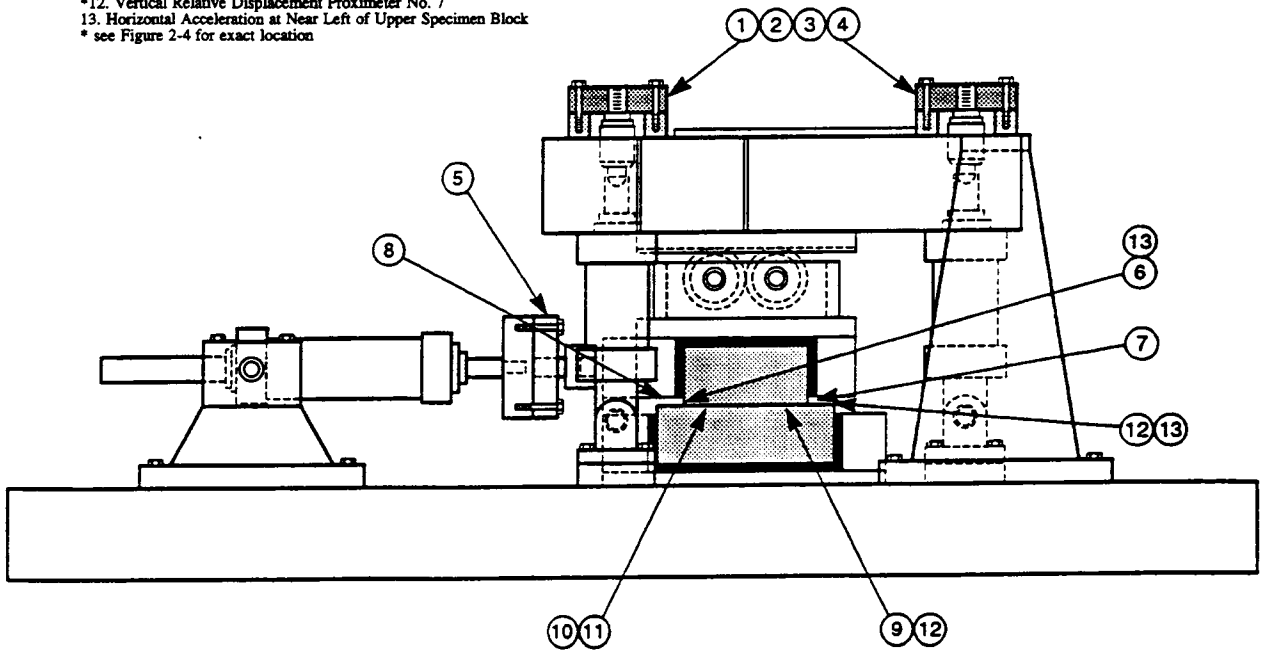

SIDE VIEW

Figure 2-1. Assembly and instrumentation diagram for direct shear test apparatus

As indicated in Figure 2-1, each of the three vertical actuators is pinned at the bottom to a clevis bolted to the base plate. At the top, each is connected to its associated load cell through a spherical coupling. This arrangement is consistent with the three degrees of freedom identified previously. Furthermore, for quick disassembly, the three actuator pins are removed, the two double flexures are detached, and the entire normal load frame, with actuators attached, can be hoisted up away from the specimen/roller box assembly.

2.1.2 Horizontal Load System

The horizontal actuator produces direct shear to the upper specimen box via the horizontal load cell, which acts through a spherical coupling. This coupling allows for slight misalignment in the horizontal shearing motion. It also allows for elevation changes of the upper specimen due to vertical load, joint surface roughness, and progressive wear. Control of the horizontal actuator load for all tests described herein was based on the horizontal shear displacement, as described in Section 2.1.3.

2.1.3 Instrumentation and Control

Instrumentation channels are identified in Figure 2-1. The locations of various relative displacement sensors on the specimen are shown in Figures 2-2, 2-3, and 2-4.

All load cells are commercially available strain gauge units with dominant sensitivity to tension/compression along one axis. Response to the applied static normal load is measured in terms of relative vertical displacements of the two blocks at four locations near the interface. Measurements near the interface are desirable to reduce the effects of slack or lack of strength in the grout. The transducers are of proximity (noncontacting) eddy-current sensing type, since horizontal movement of the two surfaces must be allowed, but only vertical displacement changes must be sensed. Hence, the four vertical measurement points can be used to resolve the rigid body displacement of the upper block relative to the lower specimen block, according to the first three degrees of freedom identified in Section 2.1.2.

Two vertical proximity transducers are mounted on each side near the joint interface as shown in Figures 2-2 through 2-4. As indicated in Figure 2-3, the specimen is grouted into the upper and lower boxes so that a 0.0254 m gap is left between the box faces. The interface, which varies from one specimen to another, is nominally enclosed within this gap. The side plates of each half of the specimen box are slotted, so that vertical proximeter supports and target plates can be mounted directly onto the sides of respective halves of the specimen near the interface. Two prongs that support each plate component are cemented into lateral holes drilled into the specimen sides. The mean elevation of these 0.00635 m thick steel components is set by gauge blocks during the cementing process, so that their positions relative to the box faces are known, as indicated in Figure 2-3. Although some movement of the specimen within the grout occurs during loading, the side slots are large enough so no interference occurs between the support prongs and the box side plates. Thus, as the upper box and associated target plates move horizontally relative to the lower specimen, change in vertical relative position is also sensed continuously. Furthermore, the heavy mounting frame for the upper box side rollers is slotted so that there is no interference between the frame and the target plates as the upper box displaces both horizontally due to shear and vertically due to unevenness and wear of the interface.

A horizontal accelerometer is mounted directly by bonding onto the upper specimen block. Thus, the accelerometer provides a measure of upper block absolute motion near the actuator attachment.

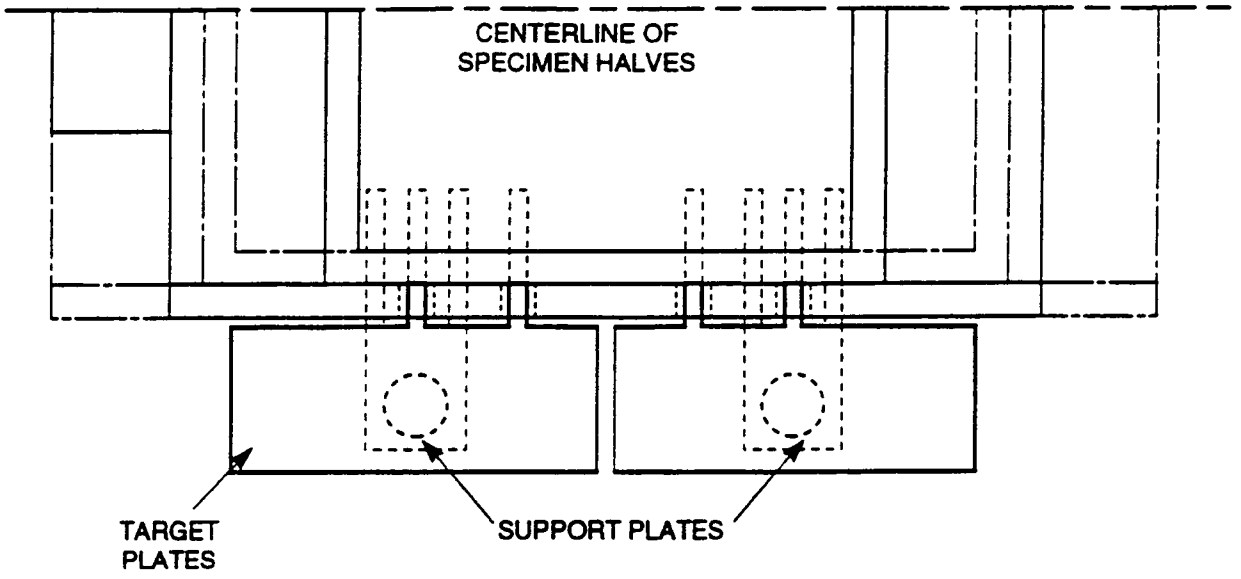

Figure 2-2. Top view of vertical displacement instrumentation supports and targets

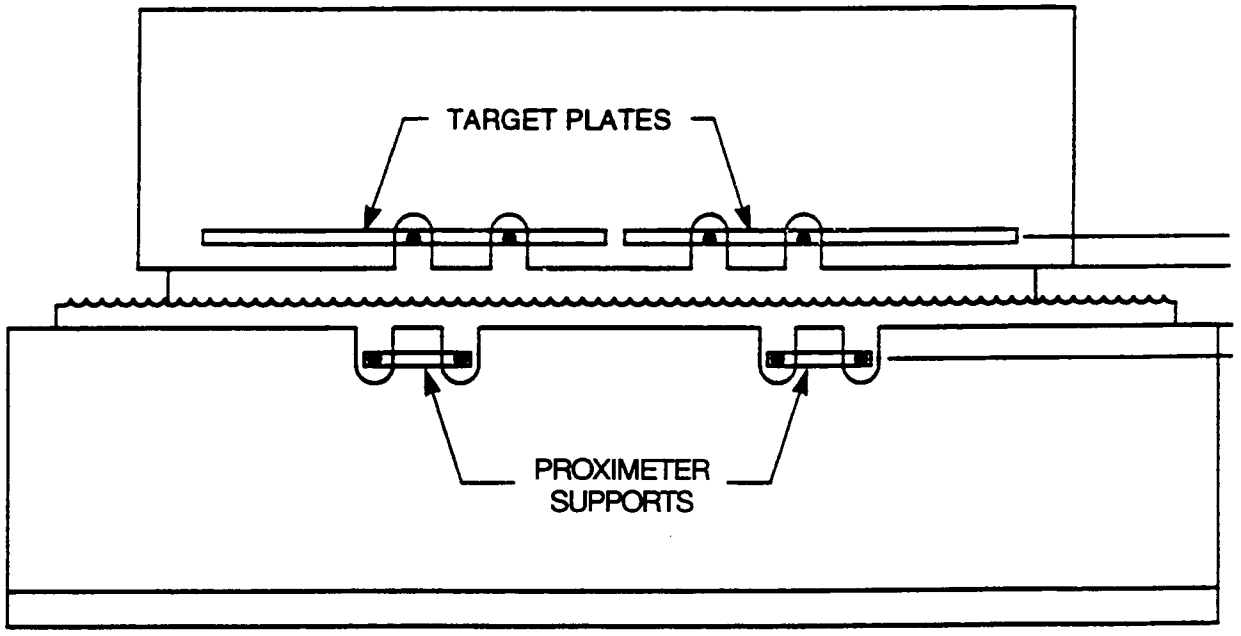

Figure 2-3. Side view of vertical displacement instrumentation supports and targets

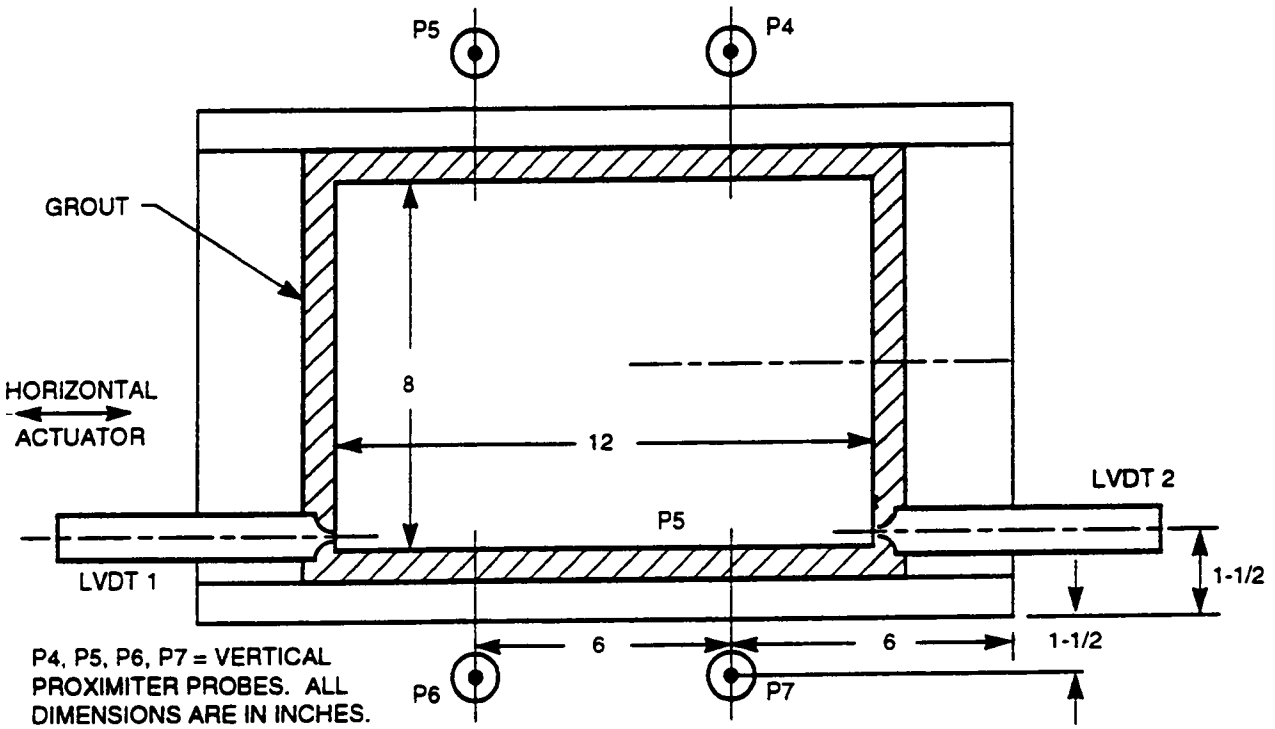

Figure 2-4. Location of relative displacement sensors on specimen lower block

Specimen block relative displacements are measured by three linear variable differential transducers (LVDT) as indicated in the various figures. LVDT1 is located at the near end of the specimen and measures displacement of the upper block relative to the lower block. Each half of the transducer is cemented directly into a hole drilled into the respective specimen block. LVDT2 is similarly mounted on the far side of the specimen pair, as shown in Figure 2-4. The outputs of these two transducers provide the direct shear movement of the joint interface. LVDT3 is mounted to sense displacement of the upper block relative to the horizontal load cell. Thus, it measures any compliance that may exist in the horizontal coupling and the grout for the upper block. The position of LVDT3 is 0.0572 m from the outside surface of the upper specimen box, on the same side as proximeters P4 and P5. This position is not shown in Figure 2-4 since only the lower specimen box is depicted.

Control in all cases was imposed on a prescribed horizontal displacement signal whose character was determined by the following options:

- Pseudostatic—A slow (20 min) ramp is applied to the relative displacement, while the force required is simultaneously recorded.
- Steady-State Cyclic—A sine wave drive signal is applied. Frequency, amplitude, and duration are based on the anticipated performance of the surface.
- Earthquake Simulation—A drive signal is generated such that a specified acceleration time history is nominally matched for a given time duration.

Calibration of load cells was performed in a commercial hydraulic apparatus with digital voltage readout. Accuracy of the load cell is within 1.0 percent of the full load. The vertical proximity eddy-current transducers were calibrated by placing the sensors in an adjustable displacement device with a micrometer head, and reading the displacement increments and associated voltages. Generally, all proximeters and LVDT provided essentially linear calibration performance in the required measurement ranges. Horizontal accelerometers were calibrated by comparison of their output with a National Institute of Standards and Technology standard accelerometer, while being excited on an electrodynamic shaker.

2.1.4 Data Acquisition System

The 13 channels of data are sampled and recorded directly on the hard disk of a 640 KB memory personal computer with a 40-MB hard disk and diskette option. This system also contains a special math coprocessor and high-speed card option. Software has been implemented that allows sampling of data at preselected rates and times, which are required by the various types of dynamic tests described above is used. Data are ultimately transferred to a diskette for further processing and plotting on other digital computers.

2.2 MODIFICATION OF BASIC APPARATUS

The basic apparatus discussed in Section 2.1 has been modified for a linear flow experiment to allow fluid to be injected into the joint at one end and to be monitored at the opposite end. Another modification is the sealing of sides parallel to the overall flow direction to confine the flow in one direction. Special modifications have also been made to the grouted faces of the specimens to prevent fluid loss. Absolute and differential pressure transducers are used to measure the inlet and outlet fluid pressures. A schematic diagram of the modified apparatus is shown in Figure 2-5. For the radial flow experiment, the basic apparatus was modified as described in Section 3.3.2.

2.3 JOINT PROFILE MEASUREMENT APPARATUS

Characterization of fracture interface required profile measurements of a rock-joint surface. The *rock profiler* is a noncontact, surface-height-gauging profilometer assembled primarily from off-the-shelf equipment (Hsiung et al., 1994). This equipment includes an Asymtek A-102B benchtop gantry-type X-Y-Z positioner and a Keyence LC-2100/2320 laser displacement meter. An LC-2320 red-visible laser head, with specified displacement measurement resolution of about 0.5 μm, is attached to the Z axis of the A-102B X-Y-Z gantry positioner.

A rock positioned beneath the A-102B gantry positioner is profiled by scanning the LC-2320 laser head across the rock surface in the X- and Y-axis directions in a raster scan pattern. The LC-2320 laser head has a measurement window of about 8×10^{-3} m from a stand off position of about 0.05 m. The LC-2100/2320 combination forms the laser displacement meter that operates on the principle of triangulation; that is, the apparent shift in the position of a laser light spot, as the laser head is raised or lowered, indicates displacement. The laser spot is quite small, about 140 μm at midrange.

The rock profiler movements were controlled by PC/AT computer commands to the A-102B X-Y-Z Table via a serial communications port. The A-102B Table had a built–in computer for interpreting high-level commands from the PC/AT and executing the moves. A custom computer program written in Borland's Turbo C, Version 2.0, was used to issue movement commands to the A-102B, to

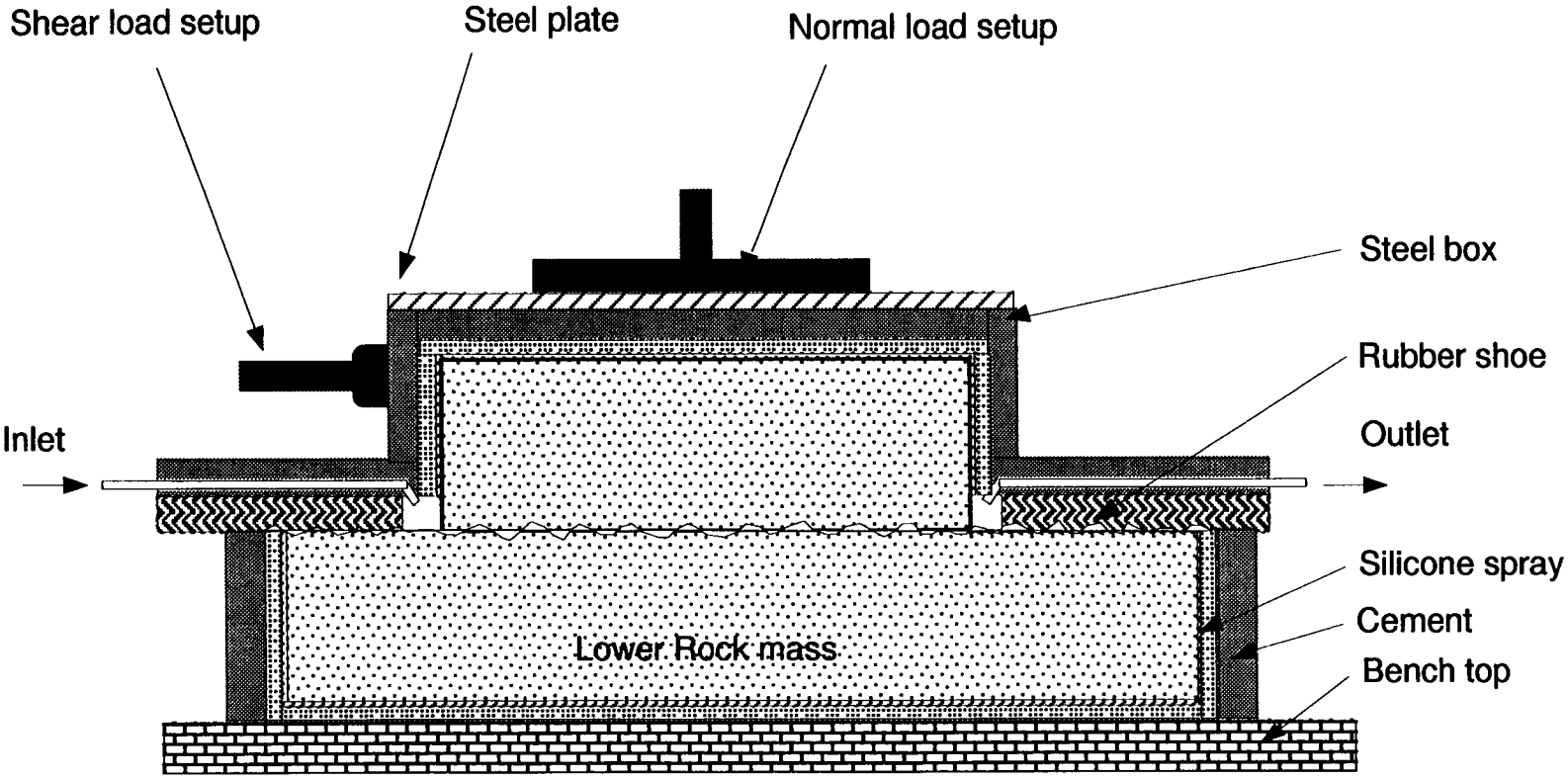

Figure 2-5. Schematic of the linear flow apparatus with normal and linear shear loading arrangements

read the displacement measurement Z-axis movement from the LC-2100, and to format and store pertinent scanning and rock-profile displacement information to a PC/AT floppy- or hard-disk data file. Additional software modifications were also made to extend the rock-profiler measurement range from 8×10^{-3} m to about 0.025 m, as the rock surface variations exceeded the originally assumed range of 8×10^{-3} m. The Z axis of the A-102B was used to accomplish this greater range. The typical performance of the integrated rock profiler is characterized in Table 2-1.

2.4 ROCK-JOINT SPECIMENS

The single-jointed welded tuff specimens were collected from Apache Leap, Arizona, as a part of Task 2 of the RM research project. The rock at the Apache Leap site is a vitrified and densely welded tuff, similar to the tuff at the proposed repository horizon at YM. The 0.4572 m (18 in.) diameter cores were collected using large-diameter core drilling technique (Hsiung et al., 1994). Rock-joint specimens with dimensions of $0.205\times0.203\times0.102$ m and $0.305\times0.203\times0.102$ m for top and bottom blocks, respectively, were prepared from 0.4572 m (18 in.) diameter cores by using a large saw at the Rock Mechanics Laboratory in the University of Arizona.

Table 2-1. Tolerance limits for rock profilometer

Maximum scan area	45.7×45.7 cm
Nominal X-Y scanning increment	1.27 mm (can be modified in software)
Z-axis range	50.8 mm
Nominal X-Y axis step	0.025 mm
Nominal Z axis step	0.051 mm
Maximum X-Y axis move error	0.76 mm (obtained by course calibration) verification grid over 30.5×30.5 cm area)
Z-axis move error	0.635 mm/50.8 mm (before scale correction)
Maximum LC-2100/2320 displacement error	0.033 mm (for a ±5 mm range from then LC-2320 center point, ranging off the smooth surface of stacked gauge blocks)
Maximum observed Z-axis repeatability error	0.0076 mm (due to homing error)
Combined Z-axis and LC-2100 linearity error	0.01245 mm standard error
Scan time	roughly 2 points per second

2.5 EXPERIMENTAL SETUP

For the linear flow experiment, the tests were conducted on a single-jointed welded tuff specimen. This specimen, consisting of upper and lower blocks with $0.0413 m^2$ (8×8 in.) of joint surface area, with the lower block having a dimension 0.0508 m (2 in.) longer than the upper block. This experiment was designed to study the effects of mechanical loading on fluid flow patterns and the joint hydraulic conductivities. The specimen halves were dried at 378 K (105 °C) for 24 hr. Then the oven was turned off, leaving the oven door closed and the rocks were allowed to cool inside the oven in order to avoid condensation in the pores. All the surfaces of the blocks, except the contacting faces, were coated with approximately 1.5875×10^{-3} m (1/16 in.) thick silicone rubber material and left at room temperature for 48 hr to cure. After the silicone was cured, the specimen halves were grouted into corresponding boxes according to the procedure described previously. Then the grout with the specimen in-place in the box was cured for 3–4 days in the oven at 327.5 K (54.5 °C). The surface profiling was accomplished by using the laser profilometer before any instrumentation was affixed to the individual boxes. After profiling, holes of different sizes were drilled onto the grouted rocks through the existing ports in the steel box and the debris was thoroughly cleaned and removed. The side instrumentation supports, target plates, and LVDT mounts in both specimen halves were then installed. The gap between the hole and the instrumentation inserts was closed with silicone rubber. Then the side of the bottom specimen along the height and the contact edges were coated with silicone rubber and a gasket made of closed cell foam and fillers was emplaced on the bottom box. The gasket channels were installed on the ends of the top box, and the input and output manifolds between channels and the rock edge were mounted. The top specimen sides and the channels were coated with silicone rubber. The rubber gasket was then installed on the upper box. A minimum of 1 hr was allowed for the silicone rubber to set. Both the upper and lower gasket-sealing surfaces were then coated with silicone grease, and the top and bottom boxes were mated. The exteriors of the upper and lower gasket halves were coated with silicone grease, and the gasket-retaining plates were bolted onto the side of the top box. After this installation, the assembly followed the sequence previously described.

In order to distribute fluid uniformly across the inlet end of the specimen, a manifold was used. The manifold consisted of 1.5875×10^{-3} -m (1/16-in.) holes 0.005 m apart drilled in a stainless steel tubing blocked at both ends. Fluid enters the manifold at its center. All these holes were aligned and pointed toward the fracture face. A tubing was split into two halves, and one half was laid against the fracture at the outlet end to ensure that the fluid would be collected from across the outlet end of the fracture. The split tube was attached to a tubing through which the fluid was drained. The inlet manifold and outlet tray are shown in Figure 2-6. The schematic for the flow loop of linear flow experiment is shown in Figure 2-7.

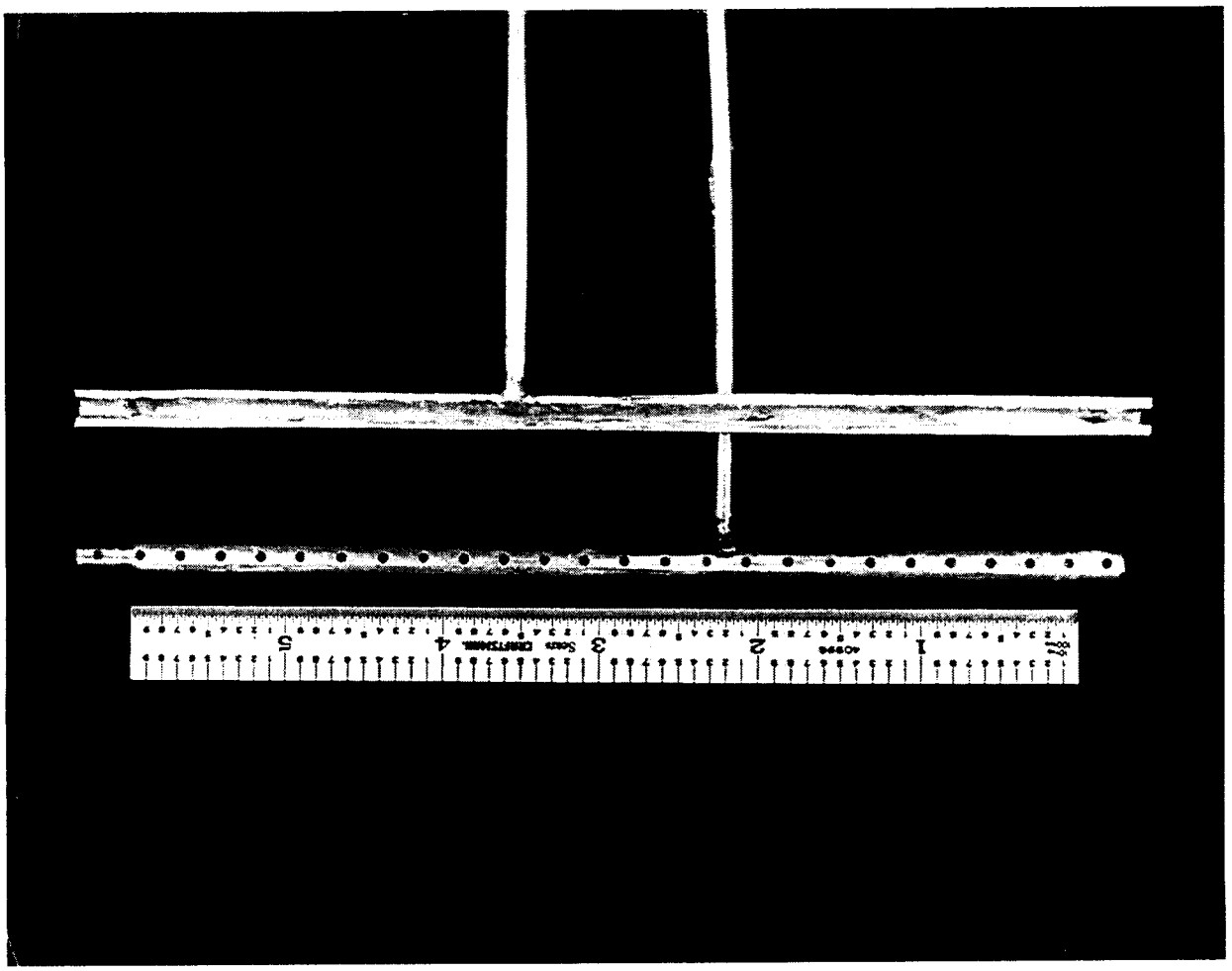

Figure 2-6. Photograph showing the inlet and outlet manifolds for the linear flow apparatus

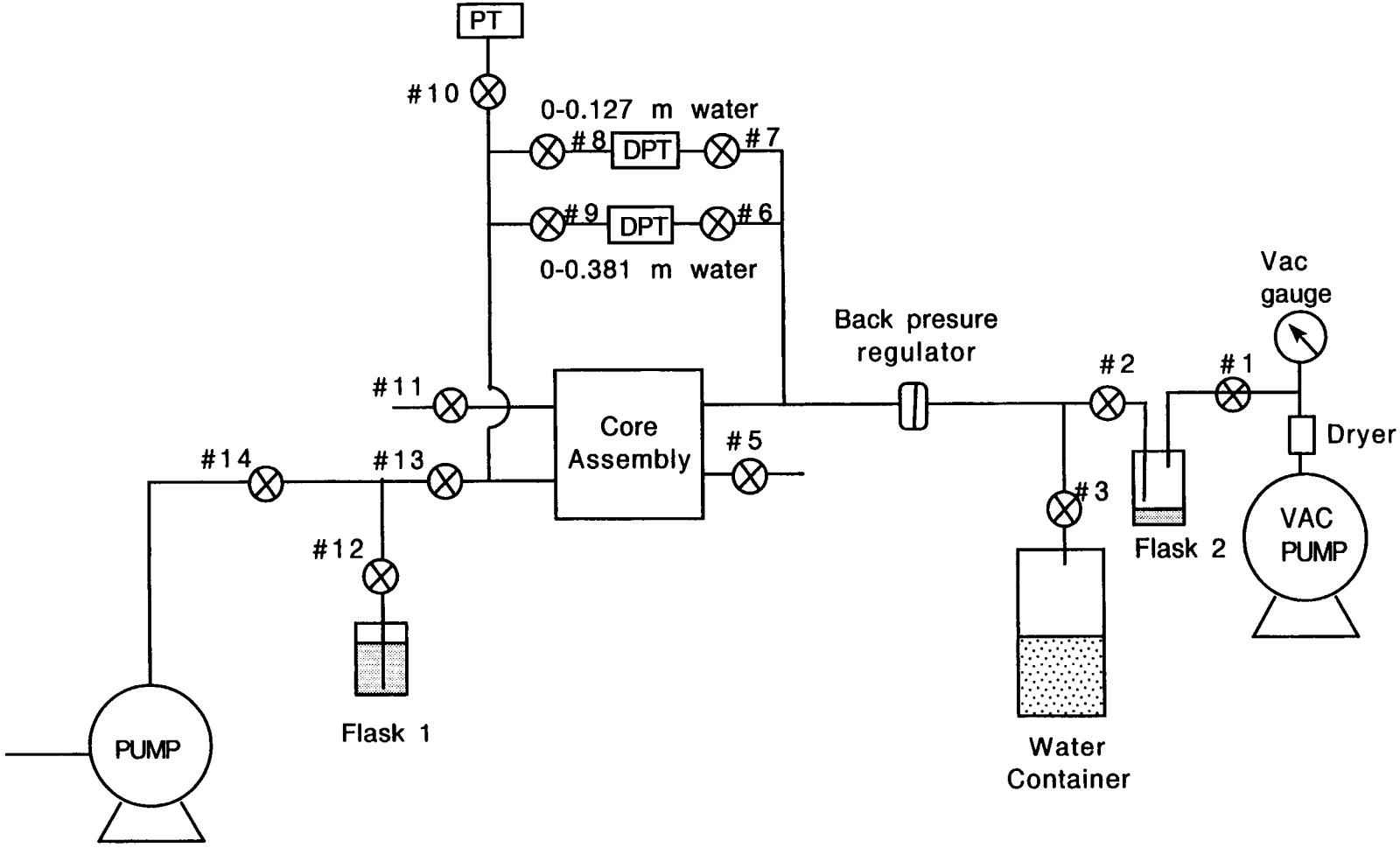

Figure 2-7. Schematic of the flow loop for the linear flow experiment

3 MECHANICAL-HYDROLOGICAL EXPERIMENTS

As the objectives imply, this study was to understand the effect of the mechanical load on the hydrologic flow conditions. The hydrologic conditions such as fluid infiltration or associated pressure drops *per se* are not expected to make any noticeable changes in the mechanical conditions of the rock because the pressure drops are too small compared to the mechanical loads. The changes in mechanical properties due to the presence of moisture in the specimen have been reported elsewhere (Hsiung et al., 1994). The focus of this study was, therefore, to investigate the effect of mechanical load conditions on the fracture fluid flow properties of the associated rock mass.

3.1 THEORY

For flow through slots of fine clearance, Buckingham reported that (Croft, 1938; Amyx, et al., 1960)

$$\Delta P = \frac{12\mu v w L}{b^2} \tag{3-1}$$

where

v	=	mean fluid velocity (m/s)
μ	=	dynamic viscosity of fluid (Pa-s)
ΔP	=	pressure drop across the fracture length (Pa)
b	=	fracture aperture width (m)
w	=	fracture cross-section width (m)
L	=	length of fracture along the flow direction (m)

In 1856 Darcy derived a purely empirical flow equation for viscous flow in porous media, which is of the form

$$q = \frac{kA(\Delta P)}{\mu L} \tag{3-2}$$

where

A = bw = fracture cross-sectional area (m^2)
k = permeability (m^2)
q = vA = volumetric flow rate (m^3/s)

Darcy's law can be derived directly from the Navier-Stokes equation by taking an average velocity of flow instead of velocities for each fluid particle, provided that inertia forces are negligible and the flow is steady state. The assumptions in Darcy's law are also inherent in the Navier-Stokes equation. Therefore, flow in a fracture can be investigated using Darcy's law. The Navier-Stokes equations are not applicable to porous media, because it is not precisely known what happens to pressures and velocities in the pores at the microscopic scale. Therefore, one must find a macroscopic law, that may be used on

the scale of the elementary domain of the porous medium, linking pressure, velocity, and external forces. Darcy's law, a phenomenological law, is precisely such a macroscopic empirical relationship.

The above description suggests that as long as Darcy's law is valid, one could equate the Buckingham equation and Darcy's law to obtain from analogy

$$k = \frac{b^2}{12} \tag{3-3}$$

In summary, the parallel plate assumption is normally used to calculate flow through a rock joint. Therefore, an experiment can be set up identical to the Darcy's flow experiment. From the application of Darcy's law, the smooth parallel plate equivalent aperture can be back calculated. It must be kept in mind that the single-aperture value used should be representative of the average of the aperture distribution between the two plates. Substituting Eq. (3-3) in Eq. (3-2) and using conventional units give

$$b = \left[\frac{12q\mu L}{w(P_1 - P_2)}\right]^{1/3} \tag{3-4}$$

where P_1 and P_2 are upstream and downstream pressures, respectively.

Darcy's law for gas flow can be expressed as

$$q_a = \frac{kA(P_1^2 - P_2^2)}{2\mu L P_a} \tag{3-5}$$

where subscript a represents atmospheric condition. The viscosity μ is determined at the mean pressure in the fracture. Then

$$b = \left[\frac{24\mu L q_a P_a}{(P_1^2 - P_2^2)w}\right]^{1/3} \tag{3-6}$$

The results presented in this report use water viscosity of 1×10^{-3} Pa-s (1 cP) and air viscosity of 1.846×10^{-5} Pa-s (0.01846 cP) at atmospheric conditions. The units for Eq. (3-6) are the same as Eq. (3-4).

Similar calculations for flow in a radial fracture geometry give rise to

$$b = \left[\frac{6\mu q \ln \frac{r_2}{r_1}}{\pi(P_1 - P_2)}\right]^{1/3} \tag{3-7}$$

where r_2 and r_1 are the external and internal radii, respectively, of the fracture.

3.2 FLOW REGIME

Transition from laminar to turbulent flow regime was inferred from the value of Reynold's number. Reynold's number is the ratio of inertia forces to the viscous forces in the flow system. An increasingly larger Reynold's number implies that as the inertia force becomes more significant, turbulence is initiated; eventually transition takes place from the laminar to turbulent flow regime. In order to circumvent the difficulties of complex flow regime, it is often of interest to conduct flow experiments under a low Reynold's number. Turbulence may be augmented by the presence of surface roughness giving rise to eddy formation. The Reynold's number representation for parallel plates is an extension of the similar representation for cylindrical pipes in the sense that the cylindrical pipe radius is replaced by an effective hydraulic radius. The Reynold's number relationship for parallel plates therefore is represented by

$$Re = \frac{vD_h}{\nu} \tag{3-8}$$

with

$$D_h = \frac{2(bw)}{(b+w)} \tag{3-9}$$

where

ν = μ/ρ = kinematic viscosity of fluid (m^2/s)
D_h = hydraulic diameter (m)
ρ = fluid density kg/m^3

For parallel plates, $b << w$ implying $D_h \approx 2b$. Equation 3-8 can be reduced to

$$Re = \frac{2\rho q}{w\mu} \tag{3-10}$$

where q = flow rate (m^3/s). The eddy formation due to surface roughness is usually represented by a relative roughness relation

$$R_r = \frac{\varepsilon}{D_h} \tag{3-11}$$

where ε is the mean height of the irregularities in the fracture (Iwai, 1976). For the gas flow experiments, the influence of gas compressibility and the Klinkenburg effect need to be accounted for.

Another representation of the Reynold's number is in its reduced form for representing flow in a fracture

$$Re^* = \frac{\rho v b^2}{\mu L} << 1 \tag{3-12}$$

where L is the typical distance between asperities. Moreover, the average aperture must be small relative to other characteristic length scales in the problem, that is:

$$\frac{b}{L} << 1 \tag{3-13}$$

While the previous equation holds for most situations of geologic importance, the latter condition may not always be true. A finite value of b/L leads to the consideration of viscous drag along the sides of the asperities (Kumar et al., 1989). In the absence of asperities, the velocity profile of the flow between two parallel plates will be parabolic. The velocity vector will be parallel to the pressure gradient.

3.3 EXPERIMENTAL PROCEDURE

The MH experiments reported herein for linear flow through rock fracture were conducted under normal and combined normal and shear loads using the specimen RM 13.2.3/13.1.2. This single-jointed welded tuff specimen was collected from Apache Leap, Arizona, as a part of Task 2 of the RM research project (Hsiung et al., 1994). Prior to conducting linear flow experiments, radial flow experiments were also conducted as described in Section 3.3.2.

3.3.1 Characterization of Rock Joint Interfaces

Prior to conducting MH experiments on the single-jointed Apache Leap tuff specimen, profile measurements were taken of both the top and bottom joint surfaces. The profile measurements were performed after the top and bottom block specimens were grouted in their respective steel boxes. After the steel box with the specimen was aligned under the rock profilometer, the computer program was initiated. The operator manually positioned the laser to define the X and Y offset for the start of the profile measurement (i.e., lower left corner of the grout box). The operator also manually defined the scanning window by moving the laser to the four edges of the rock specimen. After the four edges were identified, these parameters were stored in a configuration file, and the program then automatically scanned the entire joint surface. It was ensured that four indentations made at the four corners of the grout box were encompassed by the window. The scanning interval in both the X and Y directions was nominally set at 6.35×10^{-4} m, and the scan time was roughly 2 points/s. The total scanning time for the bottom block (0.305×0.203 m) and top block (0.203×0.203 m) took approximately 8 hr and 6 hr, respectively. After all the MH tests were conducted, joint profile measurements were again taken. For these final profile measurements, the X-Y offset and scanning window lengths were used from the initial profile so that the location of each individual scanning point was the same for both the before- and after-testing joint profiles. The joint surface profiles (i.e., height or depth of the rough surface from a fixed reference) before the initiation of the experiment are presented in the form of gray-scale and wire-meshed surface maps in Figures 3-1 and 3-2.

While surface height/depth data can be of immediate use as an indicator of surface roughness, additional data manipulation was required to retrieve aperture distribution data. One can predict the fracture permeability or effective hydraulic aperture numerically from the aperture data. Retrieval of

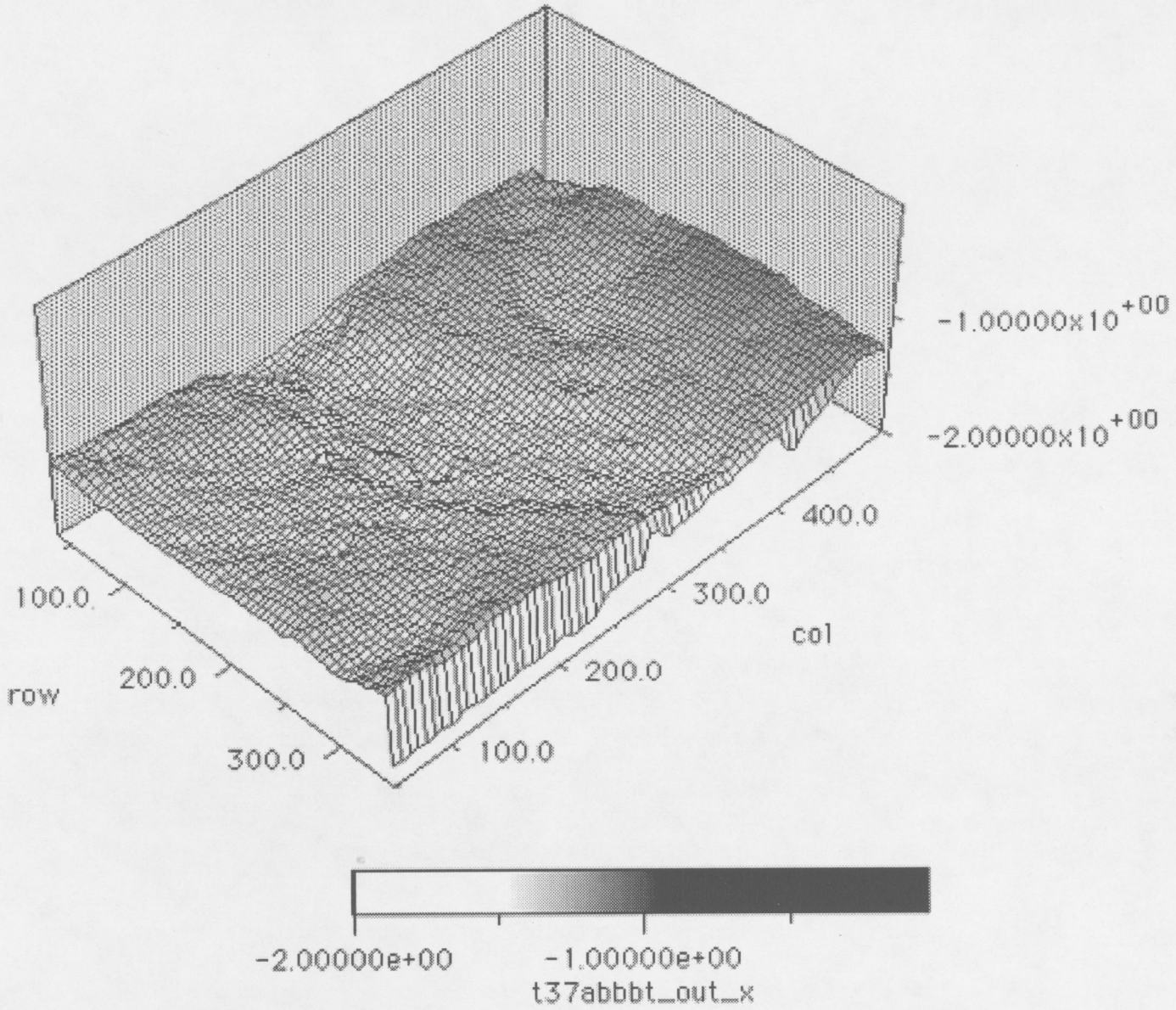

Figure 3-1. Surface profile data of the lower rock mass before the initiation of the experiment

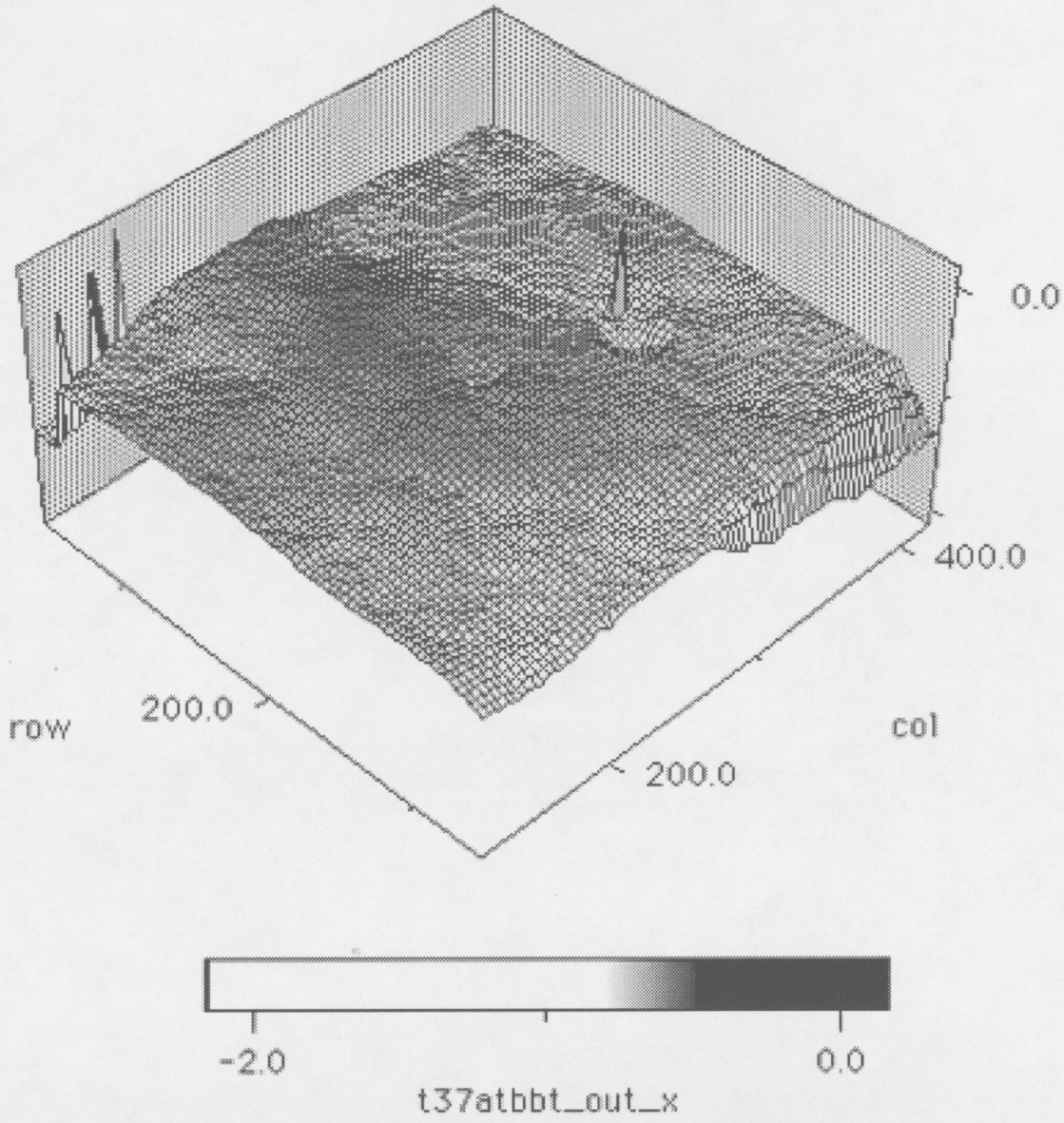

Figure 3-2. Surface profile data of the upper rock mass before the initiation of the experiment

fracture aperture data from profiled data is much more cumbersome than it seems at first. Since the apertures are typically in the submillimeter range, a slight error in positioning the rock mass under the profilometer or measurement errors reflect as large errors in the aperture data. This positioning has been complicated even more by the fact that the profiling had to be done after the rock masses were grouted into the boxes.

The numerical code FRAC_APR has been developed to retrieve fracture aperture data from fracture surface profilometry data. The two rock blocks were mated. The mating was ensured by fitting the two blocks together by moving slightly around a location approximately 0.0254 m (1 in.) from both edges of the lower blocks. The other two vertical sides were kept flush with each other at all times. As a first approximation, it was assumed that when the upper block was mated on the lower block with the grout boxes in place, the upper edges of the grout boxes facing each other would be of equal height at all four corners. A ruler with 7.9375×10^{-4} m (1/32 in.) precision was used to measure heights at all four corners. The boxes were found to be 0.0254 m (1 in.) apart at the four corners within the given precision. Although a physical mated position was easier to find, significant numerical complexities were involved when mating the two faces numerically. In order to accomplish this mating numerically, the acquired data set for the upper rock mass was inverted to match the corners of the two blocks. In essence, two grids are superimposed on each other where the upper grid was shorter than the lower grid in the X-X plane where as they are ideally expected to be of the same size in the Y-Y plane. Although the data sets contained the heights of the steel box, cement, and the rock blocks, the area covering the face of the upper block was identified first. The upper grid was positioned on top of the lower grid in such a way that the areas representing upper and lower blocks matched with each other at their lower left corners. The upper grid was then moved around, one grid block length at a time, translationally along X-X and Y-Y directions in search of the perfect mate. At each grid movement, the combined heights of the upper rock face and lower rock face as measured by the profilometer were subtracted from the distance between the bottom edges of the two grout boxes. The difference gave the aperture width corresponding to a particular position of the upper grid on the lower grid. Then the sum of the squares of differences at each grid node on the upper rock mass was determined. Then the upper grid was then moved translationally on the lower grid, and the calculation of the sum of the square differences was continued. Although the Y-Y edges of the rock masses were expected to flush with each other, about five grid-width moves were allowed in that direction. A movement of nearly 0.0508 m (2 in.) was allowed along the X-X direction. Then a minimum of the sum of the squared differences was searched. The corresponding values are presented in Figure 3-3, which represents a contour map of the sum of the squared differences. Each point on this map represents the sum of the squared difference corresponding to each movement of the upper grid on the lower grid. Interestingly, only one minimum point was observed in the search surface. The minimum point has been enlarged [Figure 3-3(b)] to ensure that the minima observed in Figure 3-3(a) was indeed the only minima. The position of the upper grid corresponding to the bottom grid was noted, and the aperture heights were recalculated. The aperture distribution thus calculated is presented in Figure 3-4. Although the search process was initiated at the extreme left corner of the lower rock mass, the minima was obtained corresponding to a position in the vicinity of the region that was expected from visual inspection.

As seen in Figure 3-2, a portion of the upper block has been chipped off near the fracture surface. Similar rock chipping was commonly observed in the rock joint at the fracture surface. It was suspected that such irregularities at the fracture edges may have contributed to reaching a spurious minima. In order to evaluate this possibility, a central grid window was selected on the upper grid in lieu of the whole grid area on the rock mass. Surprisingly, a unique minima was again obtained, even though the mating point was found to be slightly different from the former. Moreover, apertures were unusually wide on one side of the rock joint as typified by the off-blue colors. Two factors may have contributed

(A)

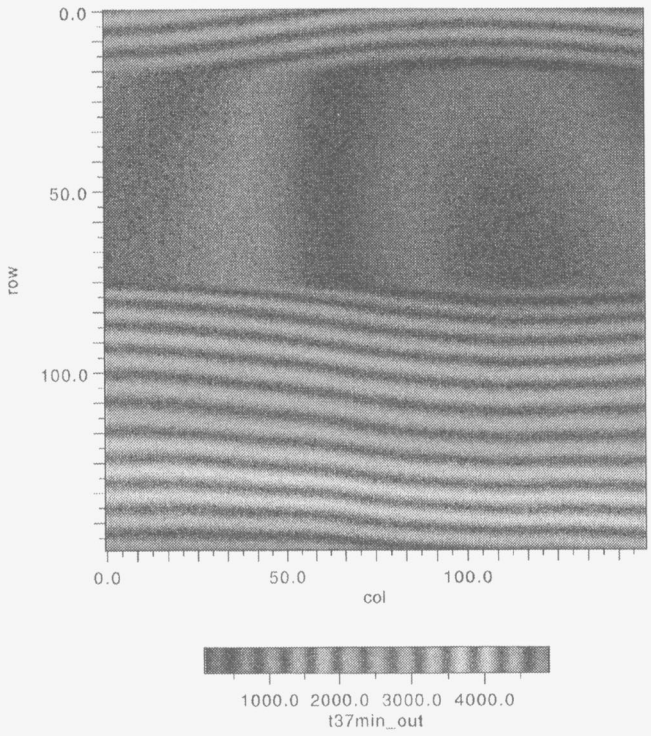

(B)

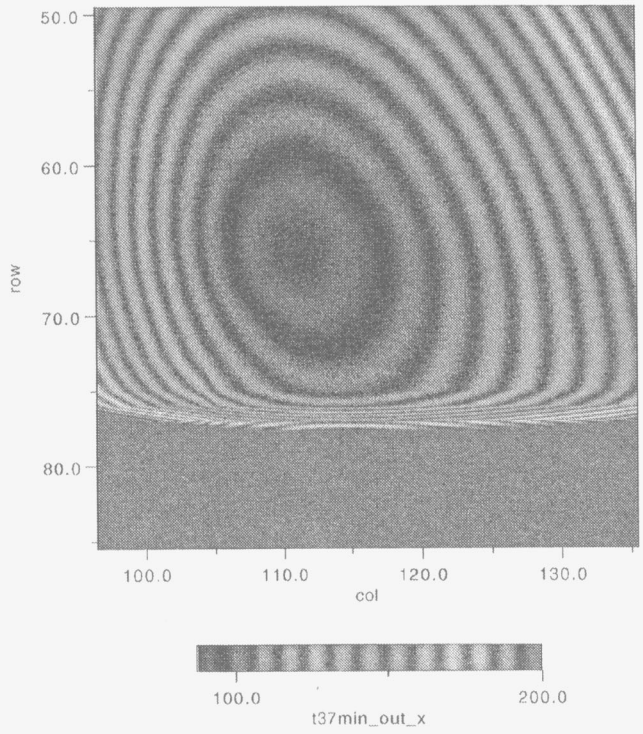

Figure 3-3. (a) Contour map of the sum of the mean square differences corresponding to numerical movement of upper block on the lower block while searching for joint mate; (b) a close-up view also demonstrates that there is only one minima

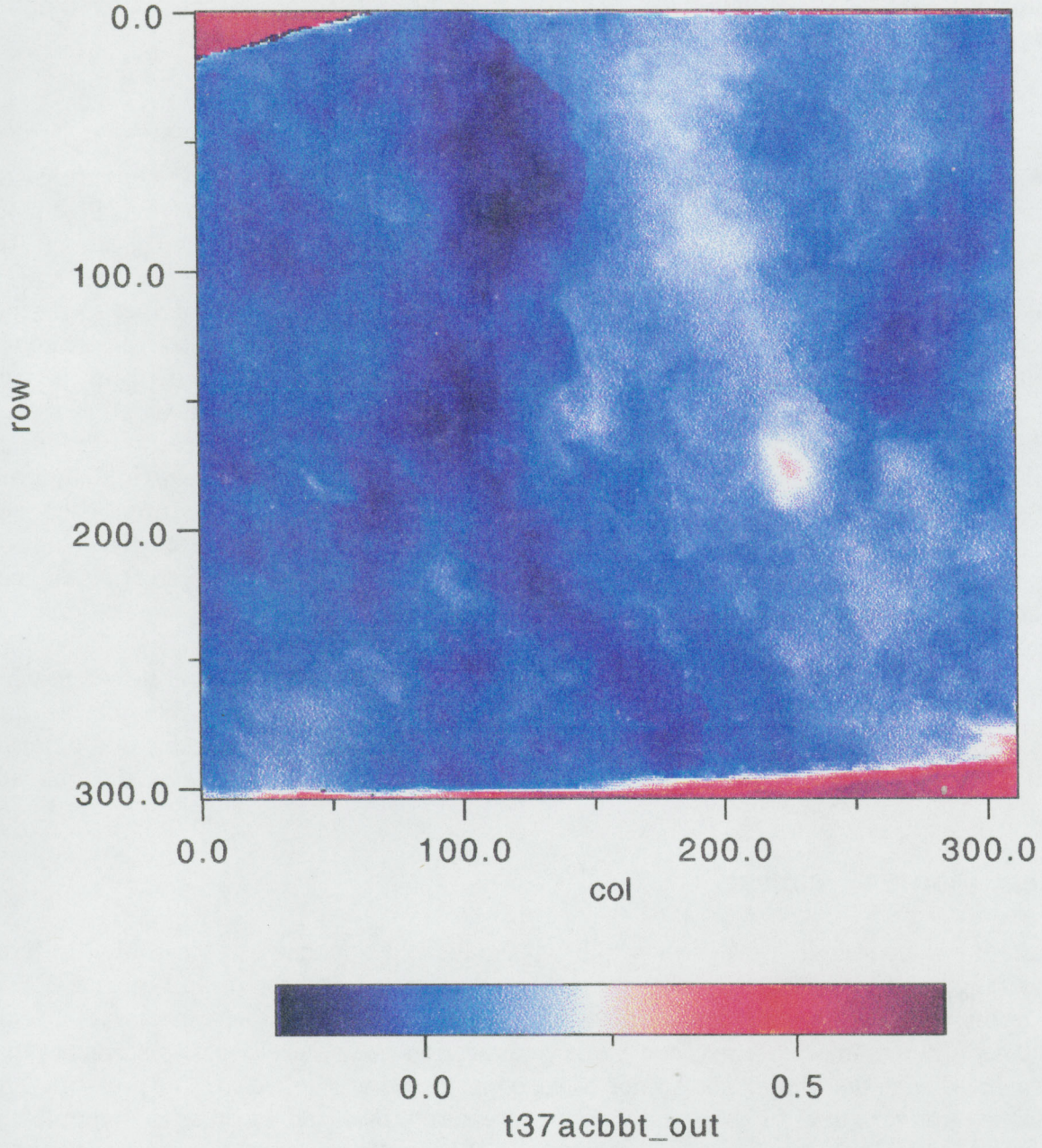

Figure 3-4. Joint aperture data obtained from FRAC_ACR computer program

to such unexpected aperture distribution: (i) the measurement of edge-to-edge distance between the top and bottom blocks may be too crude because it was measured with a ruler, or (ii) when the upper rock was placed on the lower rock in a mated condition, the normal load may have contributed to a rotary motion of the upper block thus preventing parallel alignment of the two blocks. Further work is needed to ensure a more accurate retrieval of aperture data from profilometry measurements. In Figures 3-5 and 3-6, the profilometry data for upper and lower rock masses, respectively, are presented after the joint was exposed to normal and shear loads.

3.3.2 Radial Flow Experiment

Prior to conducting the linear flow experiments, radial flow experiments were conducted with simple modifications to the joint-shearing apparatus. For this flow configuration, a hole was drilled along the axis at the center of the upper block in order to accommodate a 6.35×10^{-3} m (1/4-in.) tubing. The tubing was fixed in place by using epoxy, which also helped prevent fluid flow in the annulus between the hole and the external wall of the tubing. Figure 3-7 is a schematic diagram of the top specimen block indicating the location of the fluid injection port. The fluid was allowed to exit at the external boundary of the rock joint under the atmospheric pressure. In order to measure the fluid outflow from the joint surface, troughs were made in the grout, that were below the surface of the joint and along all four sides of the bottom block. The troughs were partitioned, and tubings were attached such that outflow from each face of the joint was collected and measured separately. Figure 3-7 also shows a schematic diagram of the bottom specimen block with attached tubings to collect and measure outflow from each side separately, assuming that one preferential flow channel at each side is identified. The outflow measurements were designed to determine how the flow changed through various preferential channels as a function of normal stress and inlet flow rate.

A flowmeter was attached to the inlet line in order to maintain a constant liquid flow rate while the normal loading across the joint was varied. A U-tube manometer was used to monitor the fluid pressure at the injection point within the joint and to record any changes due to variations in the normal loading. Applied liquid flow rates ranged between 8.33×10^{-9} and 6.66×10^{-6} m^3/s (0.5 and 400 mL/min).

3.3.3 Linear Flow Experiment

For the linear hydrologic flow method to be applicable, the apparatus was modified in terms of the sealing arrangements in order to confine the flow to one direction as shown in Figure 2-5. The faces parallel to the overall flow direction were sealed. Special modifications were necessary for the grouted faces. The fluid was injected across one whole cross section using a positive displacement pump and the fluid produced from the whole cross section of the opposite end was collected. The pressure-drop across the specimen was measured by using a differential pressure transducer. In order to determine air permeability, experiments were conducted using nitrogen (N_2) when the specimen was completely dry. N_2 was used instead of air because dry N_2 was more readily available. N_2 was injected at a constant rate from a high-pressure supply tank. The flow rate was controlled by using a pressure regulator. The pressure drop at the inlet end was measured by using a U-tube manometer and the N_2 flow rate was measured by using rotameters and digital bubble flowmeters.

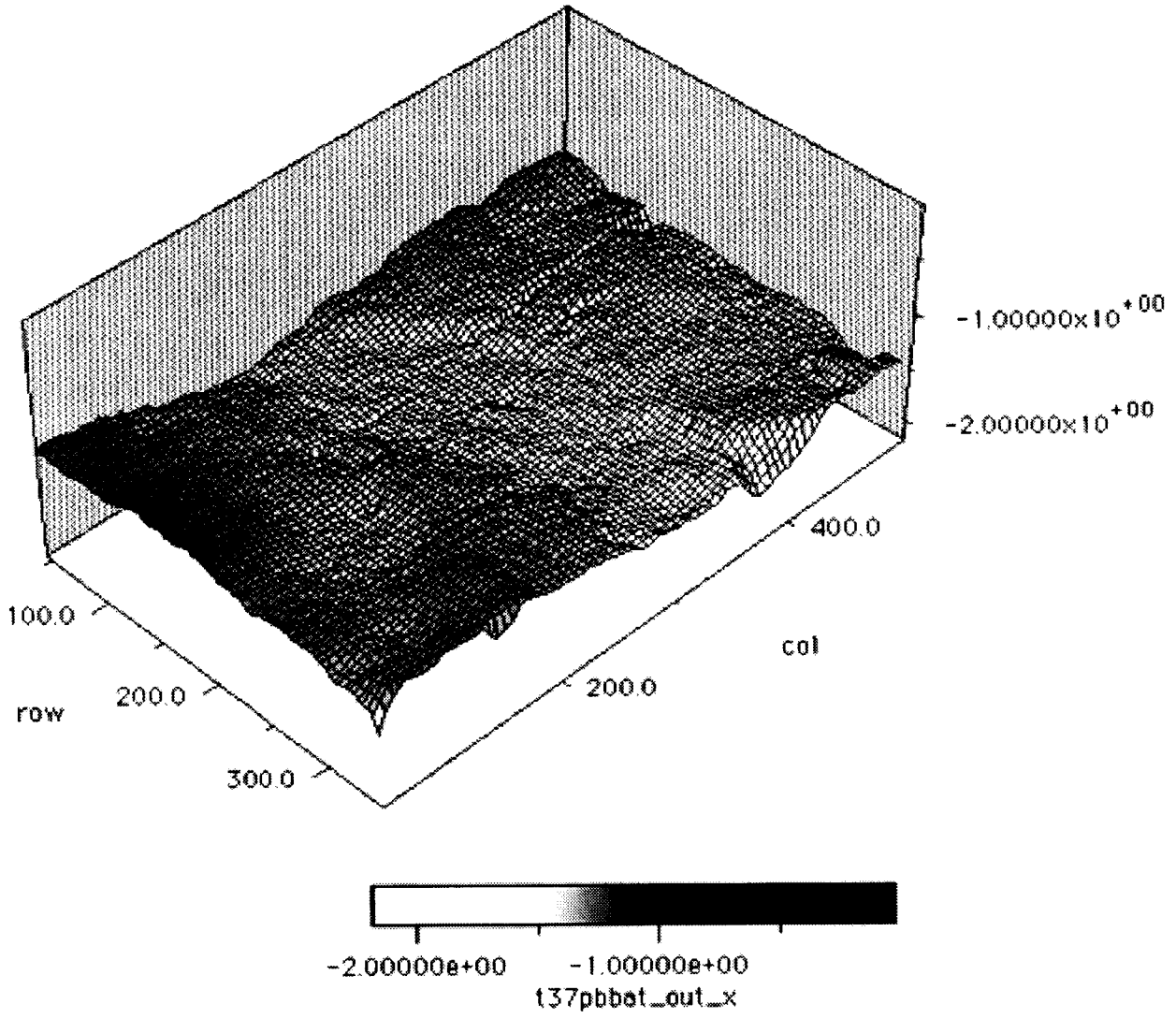

Figure 3-5. Surface profile data of the lower rock mass after initiation of the experiment

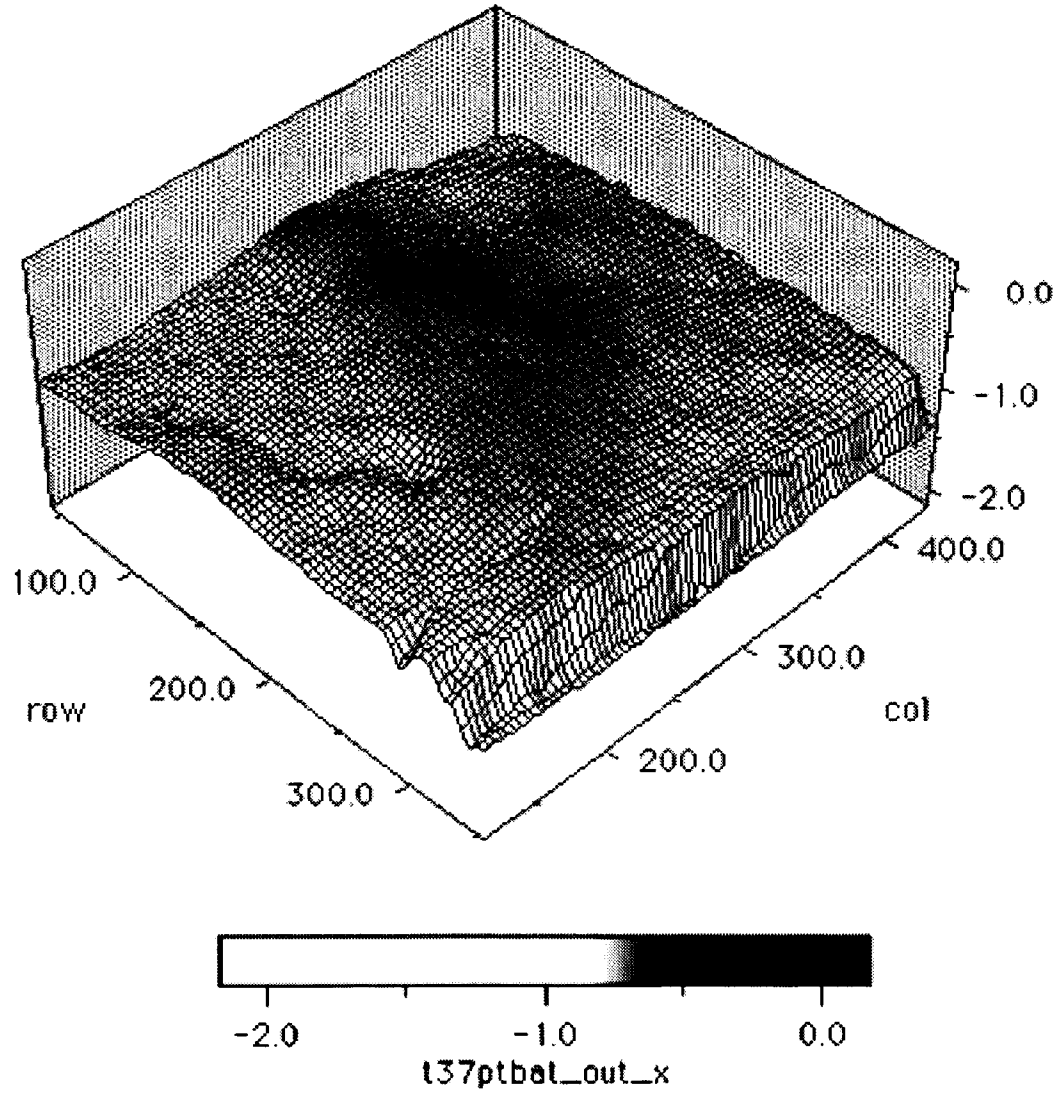

Figure 3-6. Surface profile data of the upper rock mass after initiation of the experiment

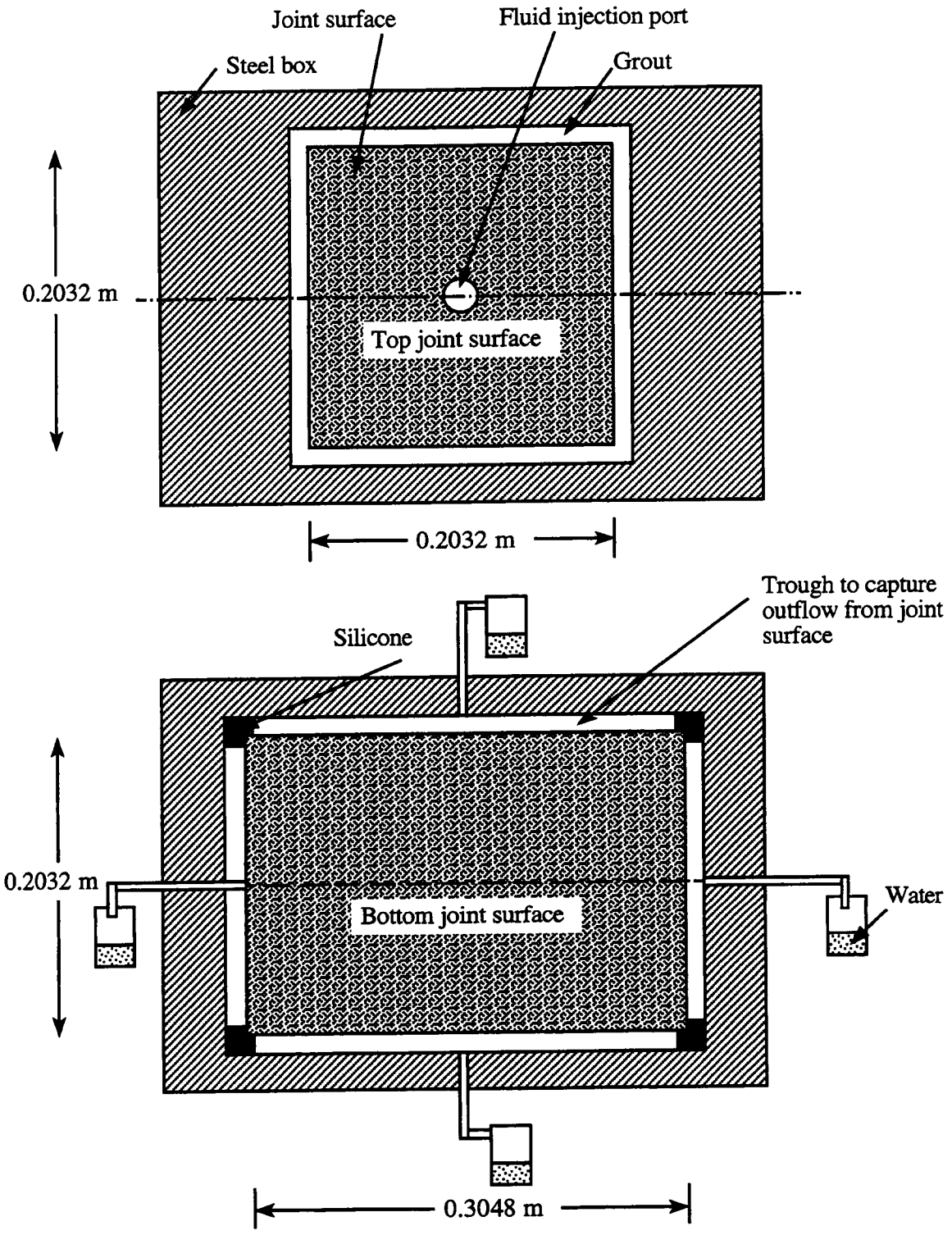

Figure 3-7. Schematic showing modification of the top and bottom block for radial fluid injection and partitioned fluid collection system

3.3.3.1 Method of Saturating Rock Specimen

In order to conduct fully water-saturated experiments, the rock specimen was evacuated *in situ* down to 744 mm Hg below atmospheric pressure by using a vacuum pump connected to the outlet end of the specimen holder. The pump was equipped with a dehydrator to prevent water vapor from entering. The specimen was evacuated for 2 hr, the inlet valve was opened, and water from an attached reservoir was allowed to be drawn into the specimen due to the existing vacuum. Excess water was collected in a flask that separated the vacuum pump and the specimen holder. Then the system was left under a positive pressure head for several days to reach pressure equilibrium. The positive pressure was obtained by shutting the downstream end valve off and maintaining the fluid reservoir at the inlet end 3 m above the specimen holder. A relative drop in the average pressure in the specimen with time has been shown in Figure 3-8 for a 1-hr time span. After this procedure, the matrix was considered to be completely saturated. However, before beginning any experiment, the specimen was evacuated for 3 to 4 min, and the above process was repeated. To ensure that the air originally dissolved in the injected water would not come out at subatmospheric pressure and create a second air phase in the fracture at atmospheric pressure, the saturation process was always followed by a high-velocity flush using the positive displacement pump.

The downstream end was connected through a tubing to a collection chamber (a large-capacity flask) placed so that there was at least 0.45 m of water remaining above the level of the fracture plane. This process ensured that the fracture would remain saturated even when no flow took place. This 0.45 m of water also ensured that air would not get into the fracture when the mechanical loading system was deactivated. It should be noted that at least 0.398 MPa pressure was applied to compress the rubber seal before the two rock faces came in contact with each other. Obviously, the dead weight of the upper loading assembly was insufficient to compress the seal materials far enough to bring the two rock faces into contact with each other. Therefore, when the load was removed after each experiment, a large void was created at the fracture plane. However, the water volume in the 0.45 m long tubing was sufficient to compensate for the increase in void space, keeping the joint specimen constantly saturated.

3.3.3.2 Flow System Modification for Shear Experiment

During the shear process, an increase in the fracture void volume was anticipated. The 0.45-m outlet end tubing once again served as a water accumulator, from which water through suction filled the additional void created during the shearing process.

In order to prevent the liquid head in the outlet tubing from falling below its entry level to the collection chamber, a three-way connector was attached to the inlet end of the specimen holder. An additional water reservoir was connected via a valve and was maintained at such a height so that water would flow at a pressure of 3 m water. The purpose of this arrangement was to avoid change in the flow rate setting of the positive displacement pump so as to compensate for the falling head in the outlet tubing when shear takes place.

3.4 RESULTS AND DISCUSSIONS

In this section, the test results from the normal load and shear displacement experiments are presented. Extensive normal load tests have been conducted, however, only limited experiments under

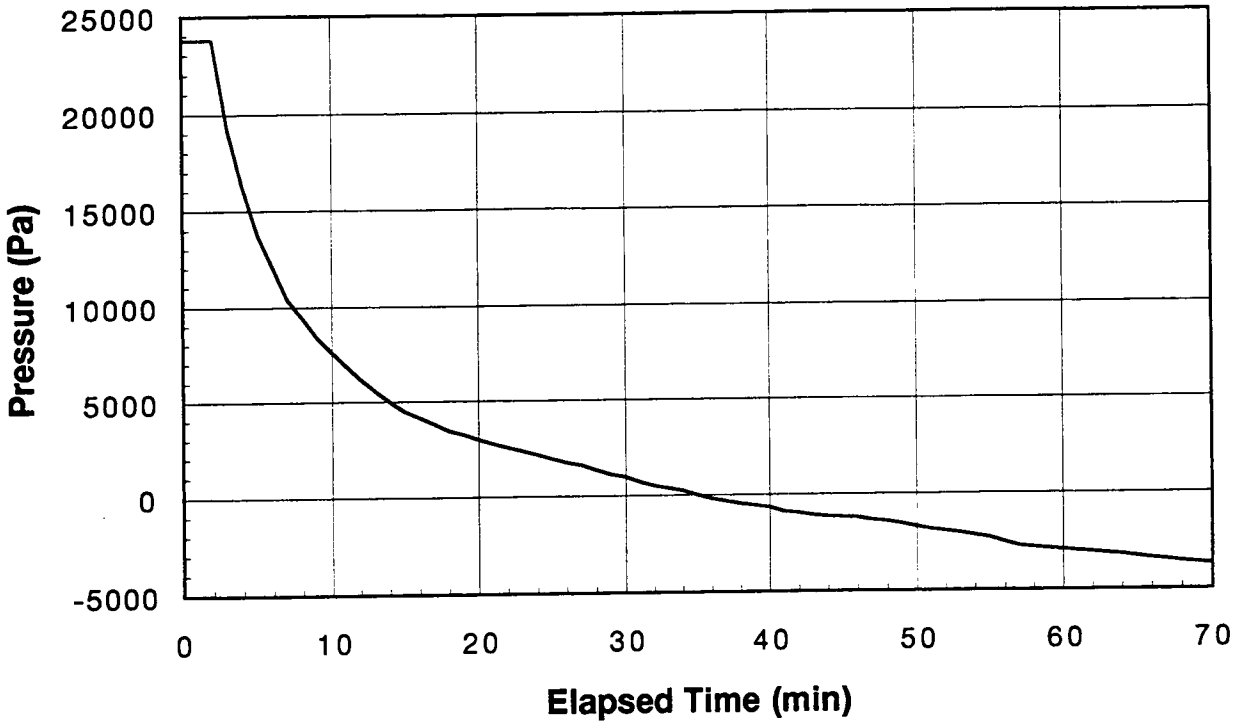

Figure 3-8. Gradual pressure losses from the fracture to the matrix indicate that the rockmass has not reached complete saturation

shear displacement were conducted. Shear displacement is a destructive method of testing and the joint samples have been destroyed. Normal load tests have been conducted using radial as well as linear flow configurations. While both water and air have been used separately as flowing fluid in the normal load experiment, only water was used as the flowing fluid in the shear displacement experiment.

3.4.1 Normal Load Experiments

In order to establish a relationship between normal stress and effective hydraulic aperture for the Apache Leap tuff, hydrologic tests were initiated. The effect of normal stress on joint closure is presented in Figure 3-9 (Hsiung et al.,1994). This figure illustrates the average joint closure measured by the four proximeters against the average applied normal stress. Each of the cycles was adjusted by subtracting the initial reading at the start of the load cycle. An important aspect of the normal closure behavior is the hysteresis and permanent set with the normal stiffness (slope) increasing much more rapidly with increasing stress. As the number of loading cycles increases, the effect of normal load on joint closure decreases (the joint behaves more elastically). Obviously, these joint closures reflect the change in mechanical aperture under normal load. Although one goal of the hydrologic experiment was to study the effect of normal load on hydraulic aperture with progressive normal load cycles, this objective could not be accomplished because the specimen had undergone many normal load cycles while conducting the instrumentation and leak tests. A maximum normal stress of 8 MPa could be applied across the joint based on the capacity of the normal load cell transducers and the surface area of the joint (0.0413 m^2). Normal joint displacement was measured using noncontacting displacement transducers as discussed earlier. Normal load tests preceded shear load tests. The readings from individual proximeters are displayed in Figure 3-10 to indicate that one end of the joint experienced a more normal displacement than the other.

3.4.1.1 Radial Flow

Air and water permeabilities of the Apache Leap tuff specimen were measured initially using a radial flow configuration. The permeability of the same specimen was later measured using a linear flow configuration. Since the upper block was shorter on each side along the length by 0.0254 m (1 in.) compared to the lower rock mass, the dimensions of the upper block served as parameters for the radial flow equation. The inner radius (r_1) of the radial flow system was taken to be the radius of the hole drilled vertically at the center of the upper because the tip of the inlet tubing did not extend all the way to the fracture plane. Since the outer edge of the rock mass was a square, the equivalent hydraulic radius of the upper block was used as the outer radius (r_2) in the flow equation.

The radial flow experiment discussed previously was designed to study the effects of mechanical loading on fluid flow patterns and the joint hydraulic conductivities. These experiments confirmed other observations that fluid flow takes place along preferential channels from the injection point to the edges of the block where it exits the joint. Such preferential flow is believed to be due to factors such as a low fluid injection rate, sloping fracture surface in the natural joints, and a spatial distribution of aperture widths. The concept of hydraulic conductivity based on Darcy's law is dependent upon the assumption of laminar flow, which requires low-water injection rates. Low fluid rates resulted in low-pressure gradients, which were harder to measure. It was, therefore, necessary to conduct experiments at higher pressure gradients. It can be observed from Eq. (3-10) that the Reynold's number is inversely proportional to the viscosity of the fluid. Therefore, one could increase the span of the laminar flow regime by increasing the viscosity at a given fluid velocity. In this case, a higher viscosity fluid made of

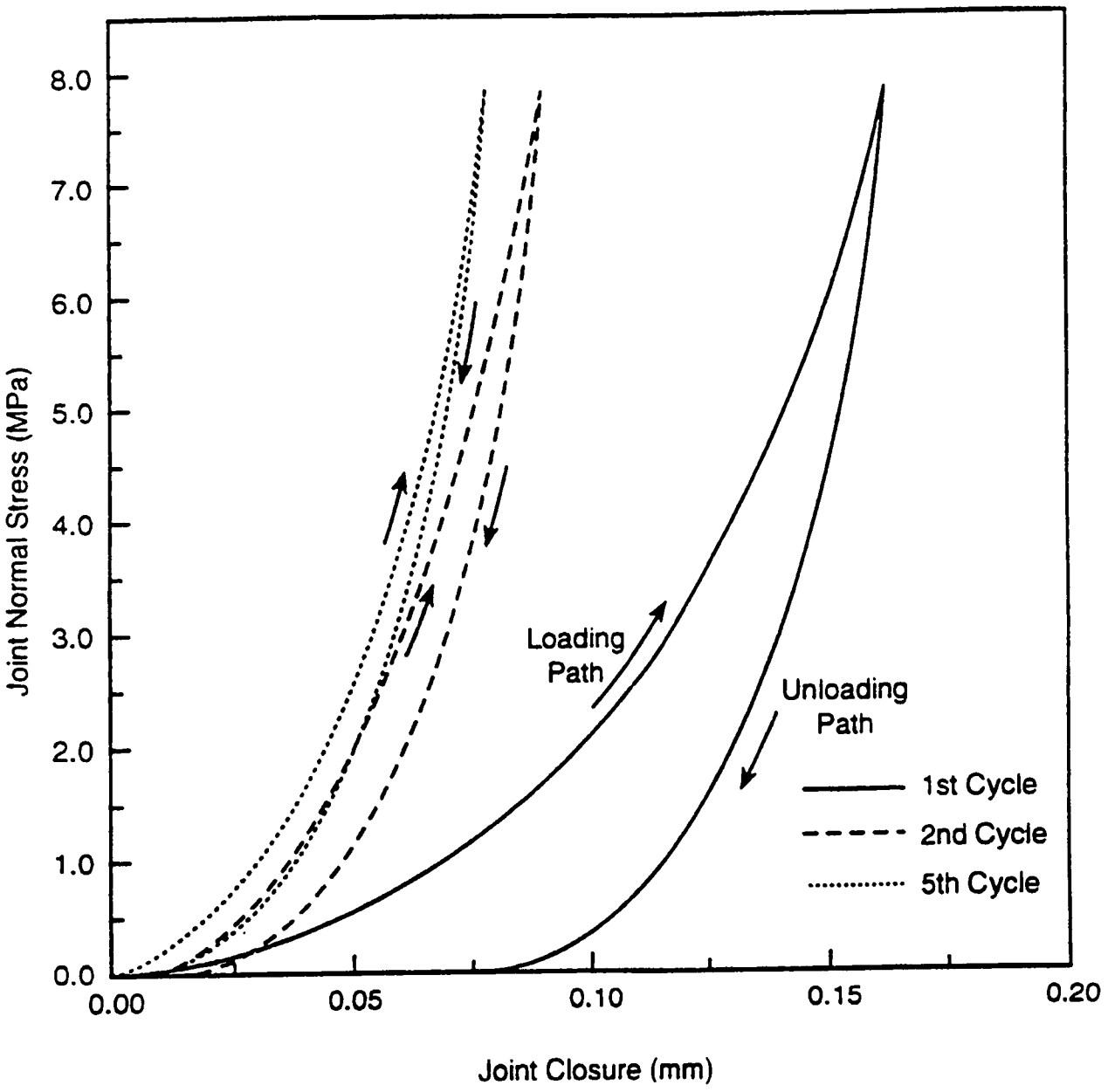

Figure 3-9. Normal stress versus closure relation for the welded tuff joint under repeated load cycles (Hsiung et al., 1994)

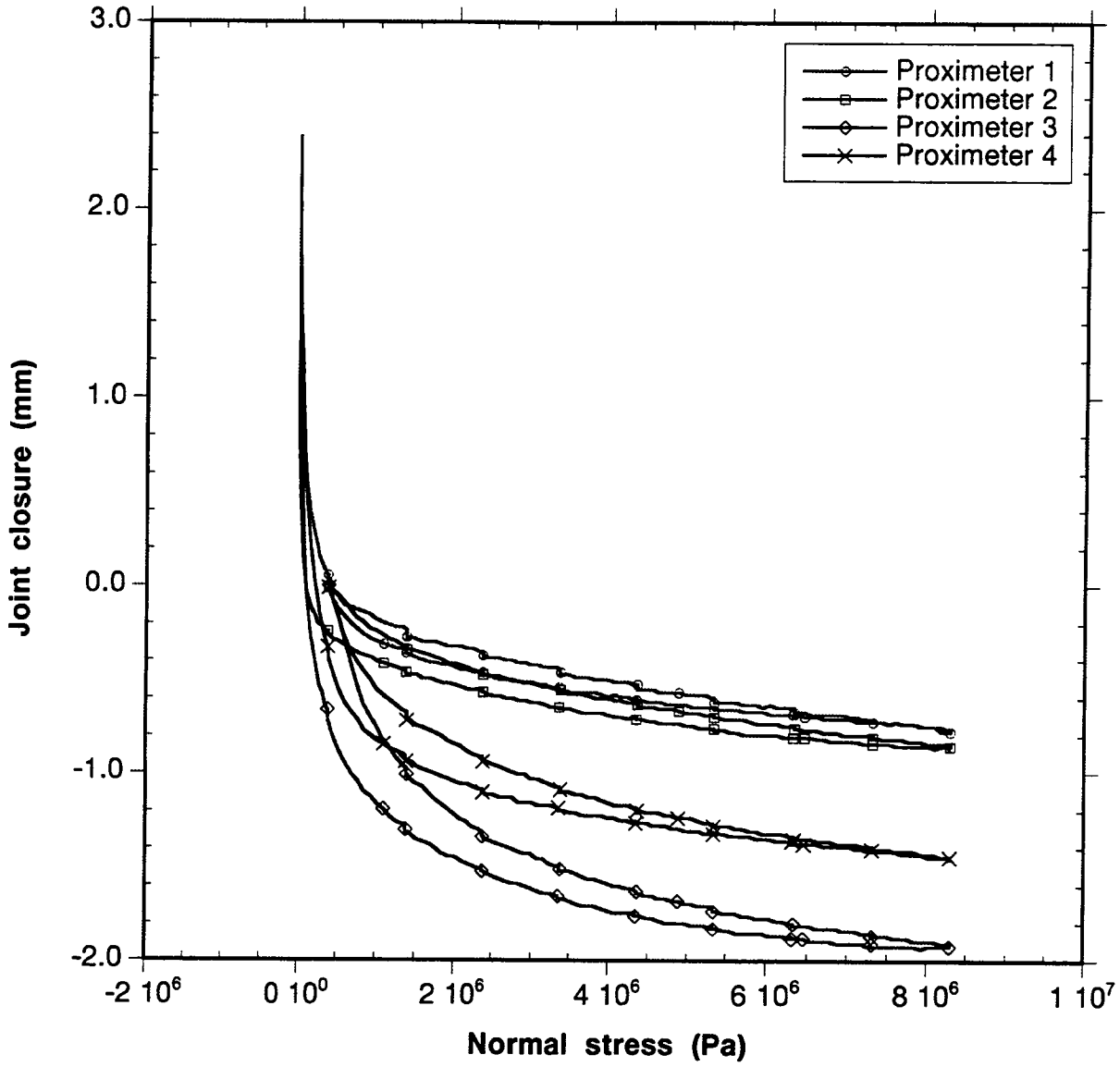

Figure 3-10. Proximeter readings versus normal load to indicate that one side of the rock has higher normal displacement than the other

a mixture of water and glycerol was used. Since permeability is a rock property, the fluid used for measurement purposes is insignificant as long as the assumptions in Darcy's law are honored. The kinematic viscosity was 1.647×10^{-5} m^2/s (16.47 cSt) at 295K (22 °C). The density of the glycerol mixture was found to be 1181 kg/m^3 (1.1810 g/mL) at 295K (22 °C). The viscosity and density were measured by using standard ASTM procedures (D 445 and D 4052, respectively). The corresponding dynamic viscosity was 1.3957×10^{-2} Pa-s (13.957 cP).

The apertures calculated at various normal stresses, using the three fluids separately, are presented in Table 3-1. Effluent volume was measured from all four sides of the specimen as shown in Figure 3-7. Liquid breakthrough was observed on all but one side. The effluent breakthrough was typically one stream per side. The stream width varied very slightly with the normal stress. Averaged over the entire test, 74.5, 18.4, and 7.1 percent of the total injected fluid were collected from the three sides. The viscosity augmentation of the flowing fluid did not make a noticeable change to the flow pattern. Despite a 14-fold increase in the viscosity of the flowing fluid, the whole joint face could not be completely saturated. Higher viscosity fluids could not be used because the pressure gradient was so low that the time required to reach steady state became extremely long. Even when pure water was used as the injection fluid, the liquid level in the manometer varied occasionally. In order to alleviate this fluctuation, the water was deaerated before injection. Although the fluctuation was reduced to some extent, the problem was not eliminated entirely. It seemed as if an air bubble was occasionally trapped at the injection port, and the fluctuation in the pressure was due to the migration of the air bubble. However, no physical evidence was found to support the air bubble migration concept. No elaborate procedure was used to saturate the rock specimen for this test. The rock specimen was saturated by flowing water through the fracture over two days. Some dry spots were clearly visible on the vertical sides of the rock specimen.

The observed channeling raises questions regarding the use of the fracture interface area for the calculation of the effective external hydraulic radius. The hydraulic radius could be obtained trivially in

Table 3-1. Effective aperture interpreted from radial flow experiments

Normal Stress (MPa)	Glycerin		Water		Air	
	Increasing Load (mm)	Decreasing Load (mm)	Increasing Load (mm)	Decreasing Load (mm)	Increasing Load (mm)	Decreasing Load (mm)
0	0.3457	0.3288	0.2729	0.2725	0.0	0.0
1	0.3148	0.2747	0.2447	0.2369	0.2532	0.2427
3	0.2789	0.2541	0.2097	0.2091	0.2175	0.2141
5	0.2661	0.2547	0.2003	0.1954	0.2057	0.2036
7	0.2510	0.2395	0.1923	0.1923	0.1972	0.1772
8	0.2432	0.0	0.1908	0.0	0.1916	0.0

the absence of channel flow. However, for channel flow, the area contacted by the flowing fluid should be used to determine the effective hydraulic radius. Unfortunately, it is not possible to measure this area without a significant redesign of the apparatus and use of highly sophisticated instrumentation such as CATSCAN or magnetic resonance imaging (MRI). As noted previously, the preferential channel flow can be attributed partly to small injection rates which are necessary to keep the fluid velocity low at the injection port. The channeling effect could not be eliminated by using higher viscosity fluids. Thus, it was necessary to implement a linear flow method so that for the same injection rate, a large cross-sectional area was available, thereby maintaining a lower velocity. It must be emphasized here that the main motivation for using radial flow in the first place was to conduct the flow experiments with minimum possible modifications to the existing direct-shear test apparatus.

3.4.1.2 Linear Flow

After steady state was established, the pressure-drop across the system was read from differential pressure transducers. Measurements were taken at various flow rates. Considerable effort was expended to ensure that various components of the experiment were performing properly. In order to ensure that the transducer was working correctly, $q \sim \Delta P$ relationship was obtained with increasing and decreasing flow rates. Sufficient time was allowed for the flow to reach steady state at each flow rate. After the method for measuring the steady-state condition was deemed correct, steady-state flow experiments were conducted at various normal load settings. At each setting, the steady state was allowed to be reached before ΔP readings were taken. A flow rate of 6.66×10^{-8} m^3/s (4 cm^3/min) was chosen on the basis of the Reynold's number requirement and was maintained at all normal loads. It should be noted that when the outlet end in a radial flow was left at atmospheric pressure, it was assumed that the inlet pressure was steady. However, the use of two absolute pressure transducers, one at the inlet and other at the outlet end of the linear flow experiment, suggested that the readings deviated from steady state as seen in Figure 3-11. This variation can be attributed to fluctuation in the power supply. Fortunately, our interest is in measuring the differential pressure as opposed to the absolute pressure. As seen in Figure 3-11, the fluctuation in the differential pressure is much less than either of the absolute pressure gauge readings.

The $q \sim \Delta P$ experimental data for air-flow experiments are presented in Figure 3-12. A linear behavior is observed up to a flow rate of 26.6 m^3/s (1.6 slpm) corresponding to a pressure drop of 4.13 kPa (0.6 psi). Above the flow rate of 26.6 m^3/s (1.6 slpm) deviation from linearity is observed and at the flow rate of 66.6 m^3/s (4 slpm) and above distinct nonlinear behavior is observed. Deviation from linear behavior indicates nondarcian flow regime.

Based on the Reynold's number calculation, a flow rate of 6.66×10^{-8} m^3/s (4 cm^3/min) was chosen for all measurements under normal load. A typical variation in pressure drop and hence hydraulic conductivity with the cycle of normal load is presented in Figure 3-13. The changes in hydraulic and mechanical aperture are presented as a percentage of the total span of change recorded between 0- and 8-MPa normal stress. The change in hydraulic aperture shows a hysteretic behavior similar to that observed in the change of mechanical aperture data. Maximum change in hydraulic aperture took place at smaller normal loads. A slight shift in the normalized aperture change data took place compared to normalized mechanical aperture data at intermediate loads. This behavior needs further investigation.

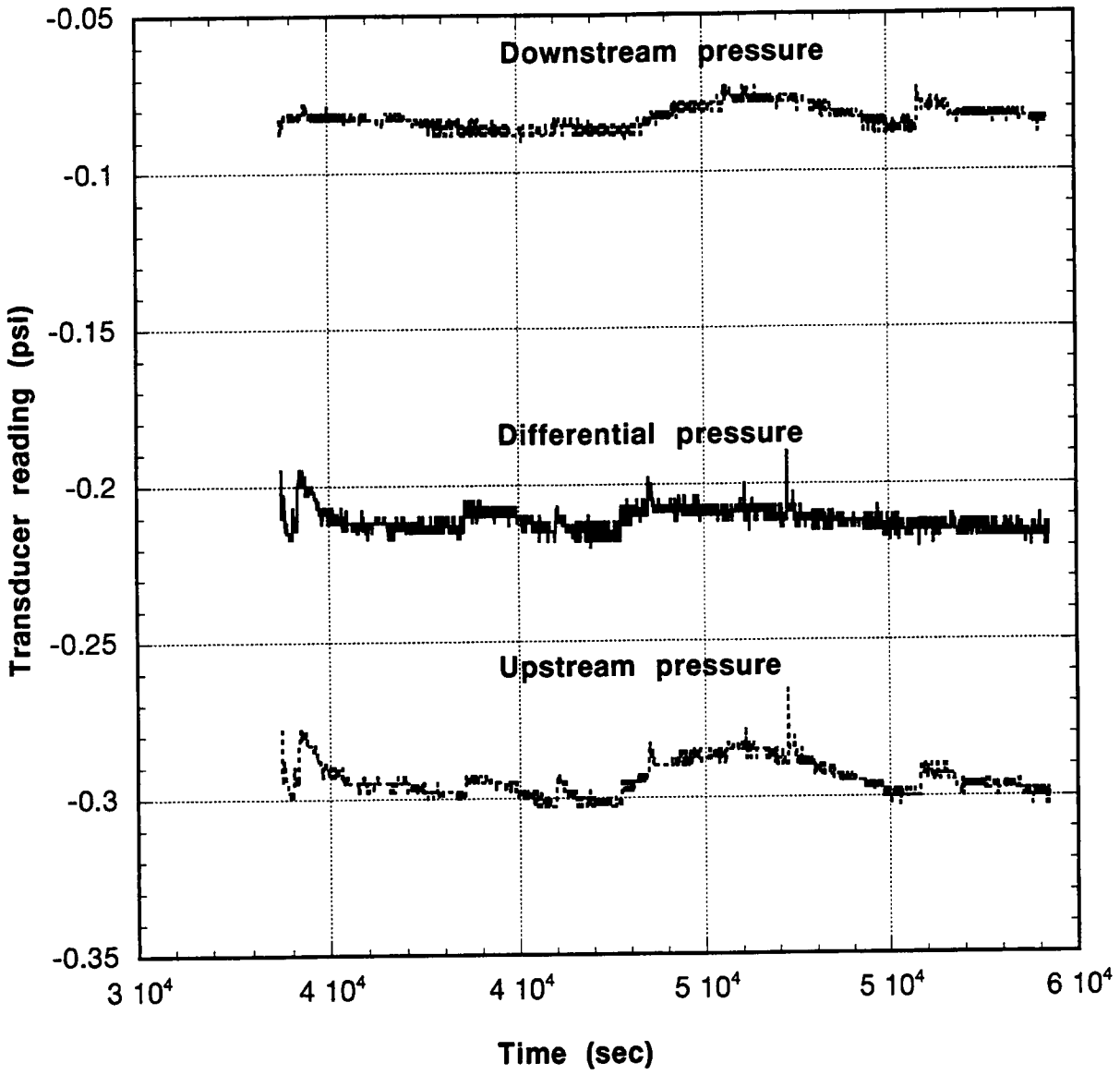

Figure 3-11. Pressure versus time plot to demonstrate the fluctuation in the absolute pressure transducer readings due to the fluctuation in power supply

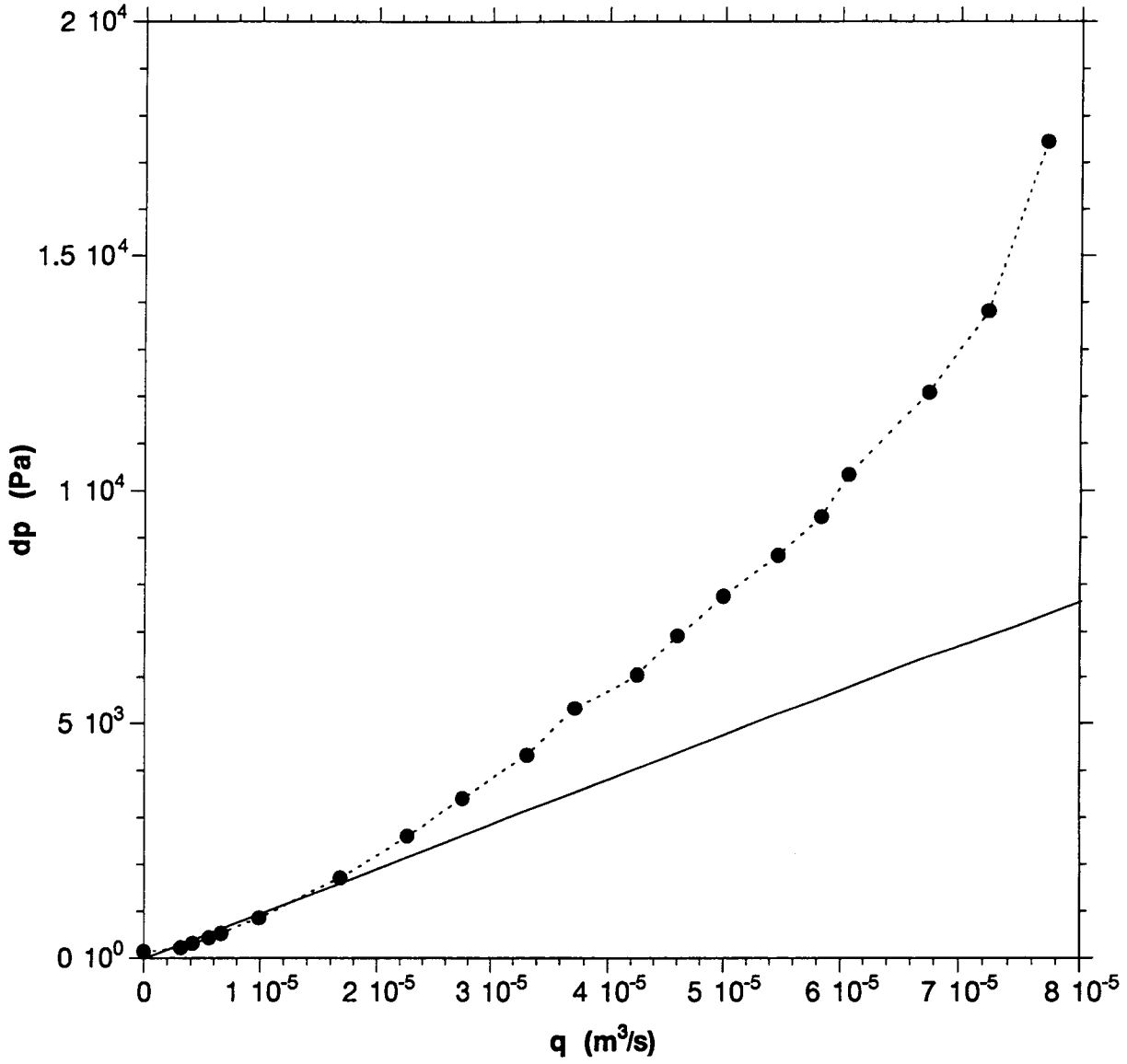

Figure 3–12. Flow rate versus pressure drop plot indicating a nonlinear relationship

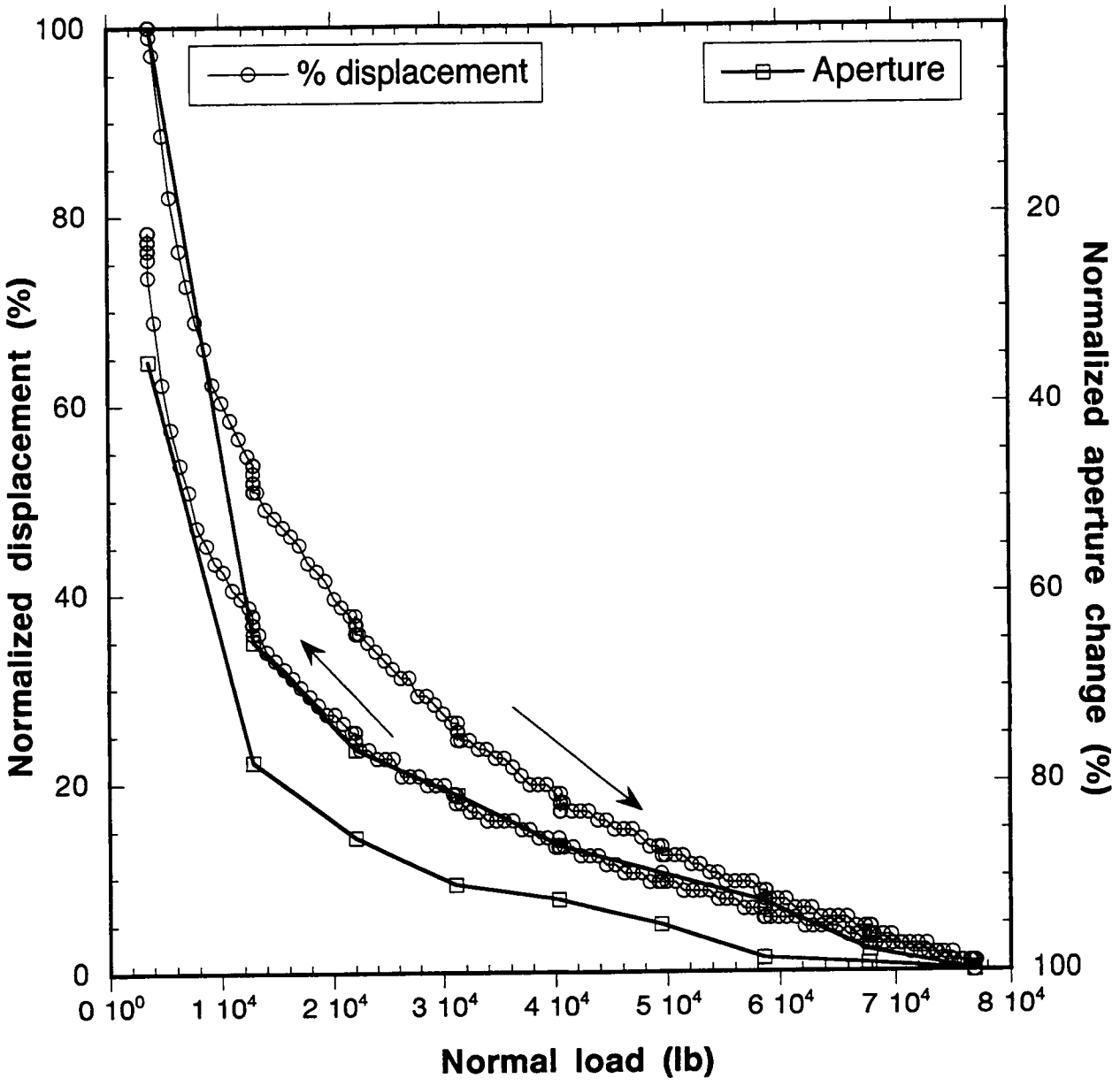

Figure 3-13. Comparison between relative change in hydraulic and mechanical aperture at various normal stresses

3.4.2 Shear Load Experiments

Only linear flow experiments were conducted under combined normal and shear loads. For the shear load experiments, 150 s (2.5 min) elapsed before moving from one load setting to another. Then data were acquired for 240 s (4 min) at each load and displacement setting. Also, 150 s (2.5 min) were allowed for a rock displacement of 6.35×10^{-3} m (0.25 in.).

The rock was subjected to four cycles of shear load under 2 MPa normal stress prior to the collection of the data presented in Table 3-2. In this table, the data are presented for conditions under 2, 4, and 5 MPa normal stress. Conducting shear experiment at more than 5 MPa normal stress would have required replacement of the horizontal actuator, which may be used for future experiments. The relationships between shear load and shear displacement are shown in Figure 3-14 for four cycles of experiments. For each cycle, the experiment was discontinued and initiated at a later date.

Test run T38HYD11.DAT was initiated but abandoned because of air being trapped in the transducer. Shear tests were conducted in test runs T38HYD12.DAT, T38HYD13.DAT, T38HYD14.DAT, and T38HYD15.DAT. Test run T38HYD12.DAT was abandoned at the end of a shear cycle at 2 MPa normal stress because a sudden rise in pressure was observed toward the end of the cycle. It was suspected that the rubber shoe of the upper grout box was obstructing flow into the collection groove. Therefore, it was decided that the reverse displacement in the shearing cycle would be limited to 1.905×10^{-2} m (0.75 in). In test run T38HYD13.DAT, surprisingly, similar pressure buildup occurred at 1.905×10^{-2} m (0.75 in.) in the reverse displacement. These pressure buildups caused leaks that were later sealed. This test run ensured the flow-path blockage was not due to the rubber shoe of the upper box, but rather to the formation of fine materials while shearing. Attempts to remove the blockage of the flow path were made by using high-velocity forward and reverse flushing. The method worked with only occasional success because the pressure in the flowing fluid was not high enough to dislodge the accumulated particles without damaging the fluid seal. Test run T38HYD14.DAT was expected to be run at 1.905×10^{-2}m (0.75 in.) shear displacement at 2, 5, and 8 MPa normal stress. Analysis of the data revealed that rock displacement did not take place at 5 and 8 MPa normal stress. Therefore, a higher capacity horizontal actuator (50,000 lb) was used. As a precautionary measure, the next test run (T38HYD15.DAT) was conducted at 2, 4, and 5 MPa normal stress.

The data presented in Table 3-2 have been measured by using water as the flowing fluid. Due to the slack in the grout box, the specified displacement always resulted in a smaller actual displacement. During the shear cycle under 2 MPa normal stress, the mean aperture was observed to be 0.1314mm with a maximum change in aperture of 39 percent. Figure 3-15 shows a vertical profile of the rock joint. This figure is not a vertical cross section, rather, each point on the fracture surface presents an arithmetic average of all the points on the fracture perpendicular to the figure. The objective is to impart an idea regarding the surface roughness at large wavelengths (i.e., large-scale surface roughness) that define the extent of change in hydraulic conductivity during shearing due to surface roughness. But the fact that the shear displacement indeed changes the fracture volume is obvious from Figure 3-16. This figure is a snapshot of the water level in the outlet end tubing (0.0127 m or 0.5 in. OD), which has fallen nearly 0.0381 m (1.5 in.). This decline suggests that the fracture volume increased by the volume equivalent to the drop in the water meniscus. At the end of the displacement cycle at 5 MPa normal stress, a maximum change in effective hydraulic aperture that could be measured of 370 percent was observed. The differential pressure transducer used in the experiment was adequate for measuring a permeability change for the specified specimen by three orders of magnitude. The absolute pressure transducers were rated at 3.45×10^{4} Pa (5 psig) pressure measurements. Therefore, the readings from these transducers were used when the pressure drop could not be measured by using the precise differential pressure

Table 3-2. Shear displacements and corresponding aperture during forward and reverse cycles at 2, 4, and 5 MPa normal stress

Movement F: Forward R: Reverse	Normal Stress (MPa)	Specified Shear Displacement m (in.)	Actual Shear Displacement m (in.)	Aperture ($\times 10^{-3}$ m)	Permeability Reduction Factor
F	2	6.35×10^{-3} (0.25)	3.23×10^{-3} (0.172)	0.12	1.0
F	2	0.0127 (0.5)	0.0105 (0.416)	0.14	0.9
F	2	0.01905 (0.75)	0.0166 (0.656)	0.14	0.9
F	2	0.0254 (1.00)	0.0227 (0.894)	0.15	0.8
R	2	0.01905 (0.75)	0.0161 (0.633)	0.14	0.9
R	2	0.0127 (0.50)	0.0093 (0.386)	0.13	0.9
R	2	6.335×10^{-3} (0.25)	0.0036 (0.141)	0.10	1.3
F	4	6.35×10^{-3} (0.25)	0.0036 (0.142)	0.09	1.3
R	4	0.01905 (0.75)	0.0167 (0.661)	0.15	0.8
R	4	0.0127 (0.50)	0.0109 (0.431)	0.13	0.9
F	5	0.0127 (0.50)	0.007 (0.28)	0.04	3.5
R	5	0.0254 (1.00)	0.0184 (0.725)	0.18	0.7
R	5	0.01905 (0.75)	0.0172 (0.679)	0.15	0.8
R	5	0.0127 (0.50)	0.0114 (0.449)	0.04	2.9

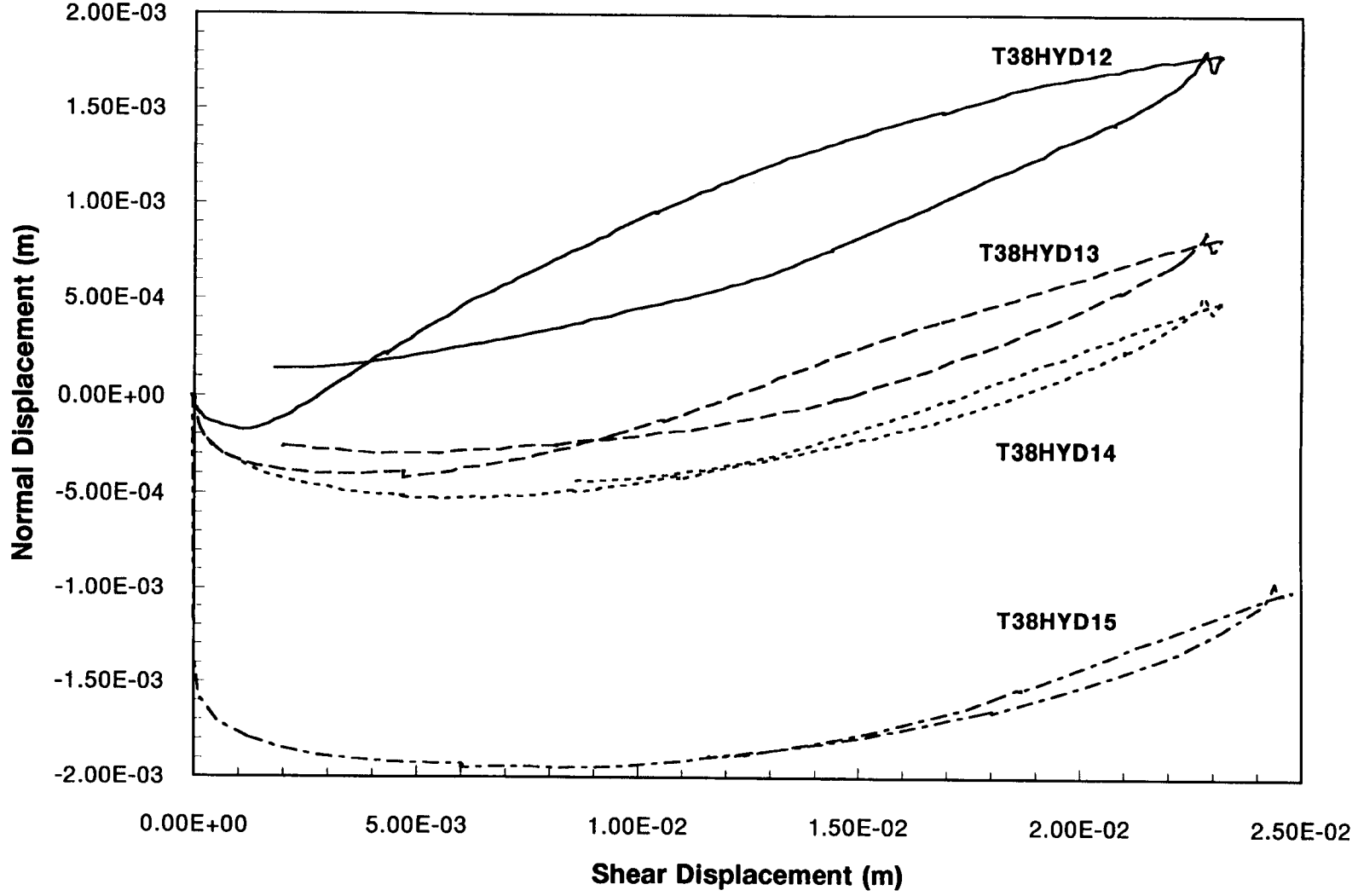

Figure 3-14. Shear stress versus shear displacement during four cycles of 2 MPa normal stress

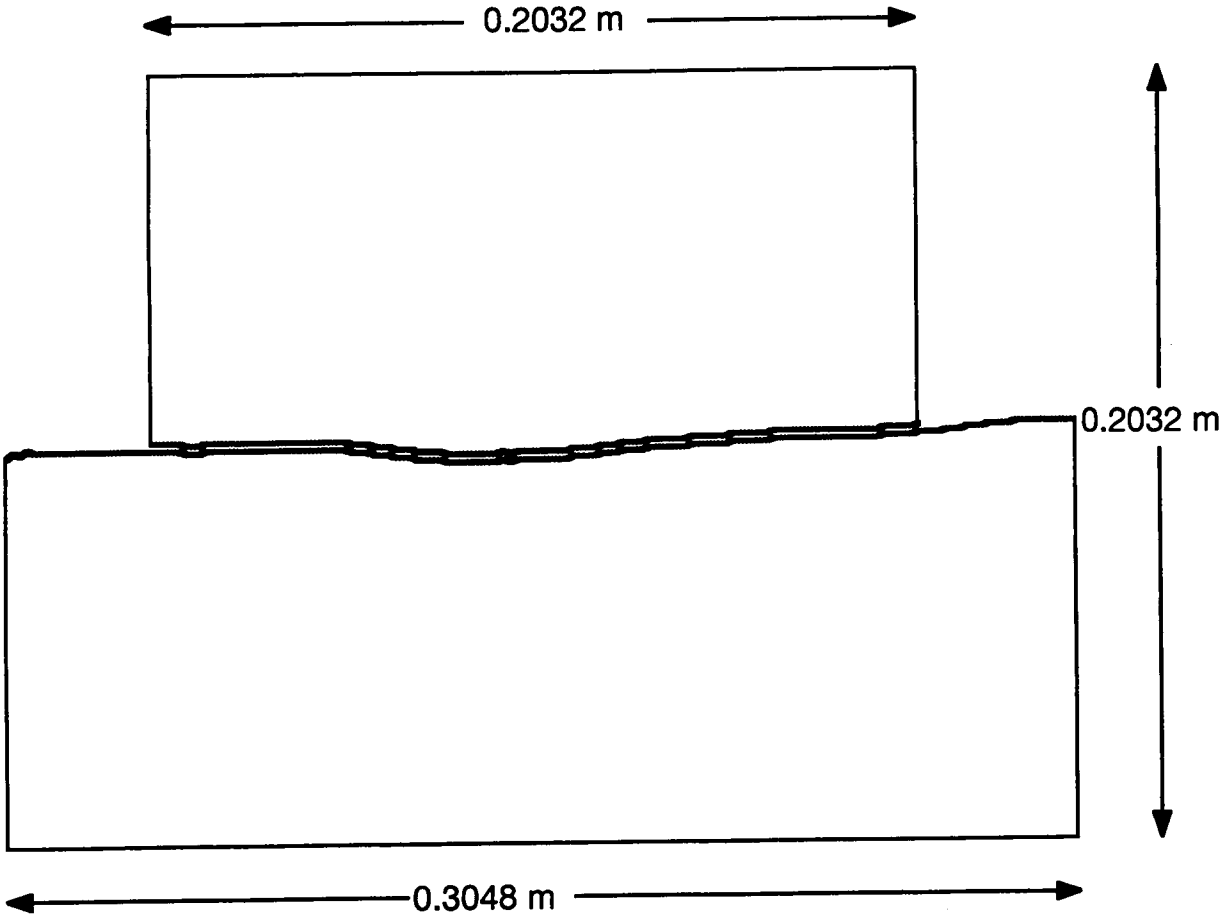

Figure 3-15. One-dimensional fracture with a resolution of 512 nodes/m

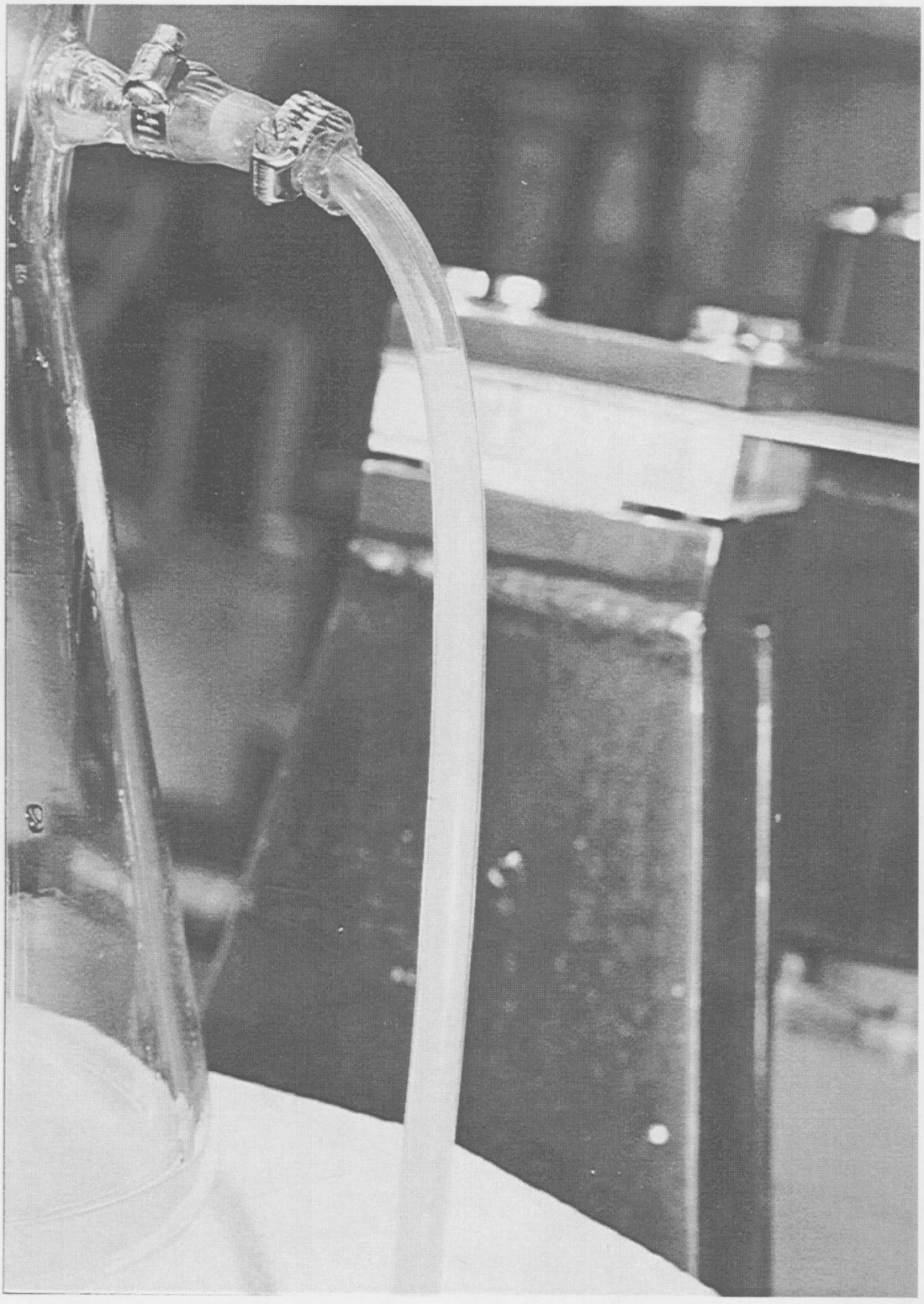

Figure 3-16. Photograph showing drop in liquid level at the outlet end after shearing when fluid injection had been stopped

transducer. The shear displacement values at which the absolute or differential pressure exceeded the calibrated range are designated as having been caused by the constriction. Adding pressure transducers with a higher range would not have improved the apparatus because the sealing inside the grout box was rated at only 6.9×10^4 Pa (10 psig). From the pressure transducer in the positive displacement pump, it was observed that during the constricted flow pressure easily built up above 6.9×10^4 Pa (10 psig). Figure 3-17 shows a scheme for the shear displacement. In this scheme, the upper rock was not allowed to come back to the zero position because the rubber shoe at one end of the upper rock mass was suspected of blocking the outflow channel and thus raising the constricted flow effect. The rubber shoe was later proven not to cause the constricted flow effect. The gray areas without remarks indicate the normal and shear load setting at which the experimental data were successfully obtained. The data that were collected under leaks or constricted flow effect were discarded. It is observed that most bad leaks occurred at the end of the forward and at the beginning of the reverse cycle at 4 MPa and 5 MPa normal stresses. The constricted flow effect due to the production and accumulation of fine particles did not occur in any definite pattern. Attempts had been made to dislodge the blockage of flow through reverse flushing. This procedure helped clear the flow paths in only a few instances. The migration of fine particles under a steady-state flow condition can be observed in Figure 3-18. At the end of the steady-state experiment at each displacement, particle accumulation was removed by lowering the exit end of the outlet tube, tapping the tube, and flow from the water reservoir to dislodge the accumulated fine particles. Figure 3-19 gives evidence of the dense deposit of the dislodged fine particles in the joint while flushing the deposits at the outlet valve. Figure 3-20 clearly shows a slug flow settling pattern of the fine deposit that could have affected the steady state flow measurements. Therefore, data acquisition was interrupted until the hydrologic conditions were suitable for the steady-state runs after flushing. Fortunately, at the water injection rate of 6.66×10^{-8} m^3/s (4 cm^3/min), there was no significant suspension of particles in the flowing fluid. Thus, change in water viscosity was not considered significant. Figure 3-21 shows the liquid pressure drops for 2, 4, and 5 MPa normal stress experiment cycles with shear versus vertical displacement in the background.

At the end of the experimental, the experiment apparatus was dismantled in order to visually inspect the changes in the rock joint. A much larger amount of fine deposits was observed in the joint than could be interpreted from the amount of fine deposits migrating during the flow experiment. The fine particles existed as a thick paste. It could not be determined if these fine particles existed in the same thick paste form during the flow experiment or if the drying of water before the dismantling of the apparatus gave a paste-like texture to the fines aggregate (Figure 3-22). The rock surfaces were allowed to dry under room temperature and then the fine particles were collected for further analysis. The fines that migrated with flowing fluid were collected along with the effluent. Then the effluent was evaporated in a constant temperature oven to recover the solids. A total of 3.81×10^{-2} kg of fine solids were dislodged from the rock during four displacement cycles under normal stresses of 2 MPa, and one cycle at 4 and 5 MPa each, over a displacement of approximately 1.905×10^{-2}m (0.75 in.). The texture of the dried fines can be seen in Figure 3-18.

The modification of the apparatus for confining pressure performed as expected during both normal and shear load experiments. However, the leaks that impaired data acquisition at a few shear displacement increments were caused by the slack distortion of the grout box while shearing. In order to facilitate the grouting process, the boxes were constructed of steel plates held together by bolts. It was observed that during the shearing process, the bolted plate interfaces opened up, causing severe leaks. The 1.5875×10^{-3} m (1/16 in.) thick silicone coating on the rock block separating the rock from the cement did not work as desired to prevent leaks. It is likely that the severe shearing process to which the silicone rubber seal had been subjected punctured the seal, causing leaks to develop. However, these leaks stopped after the displacement was complete, except in some cases. Since a sufficient head of water

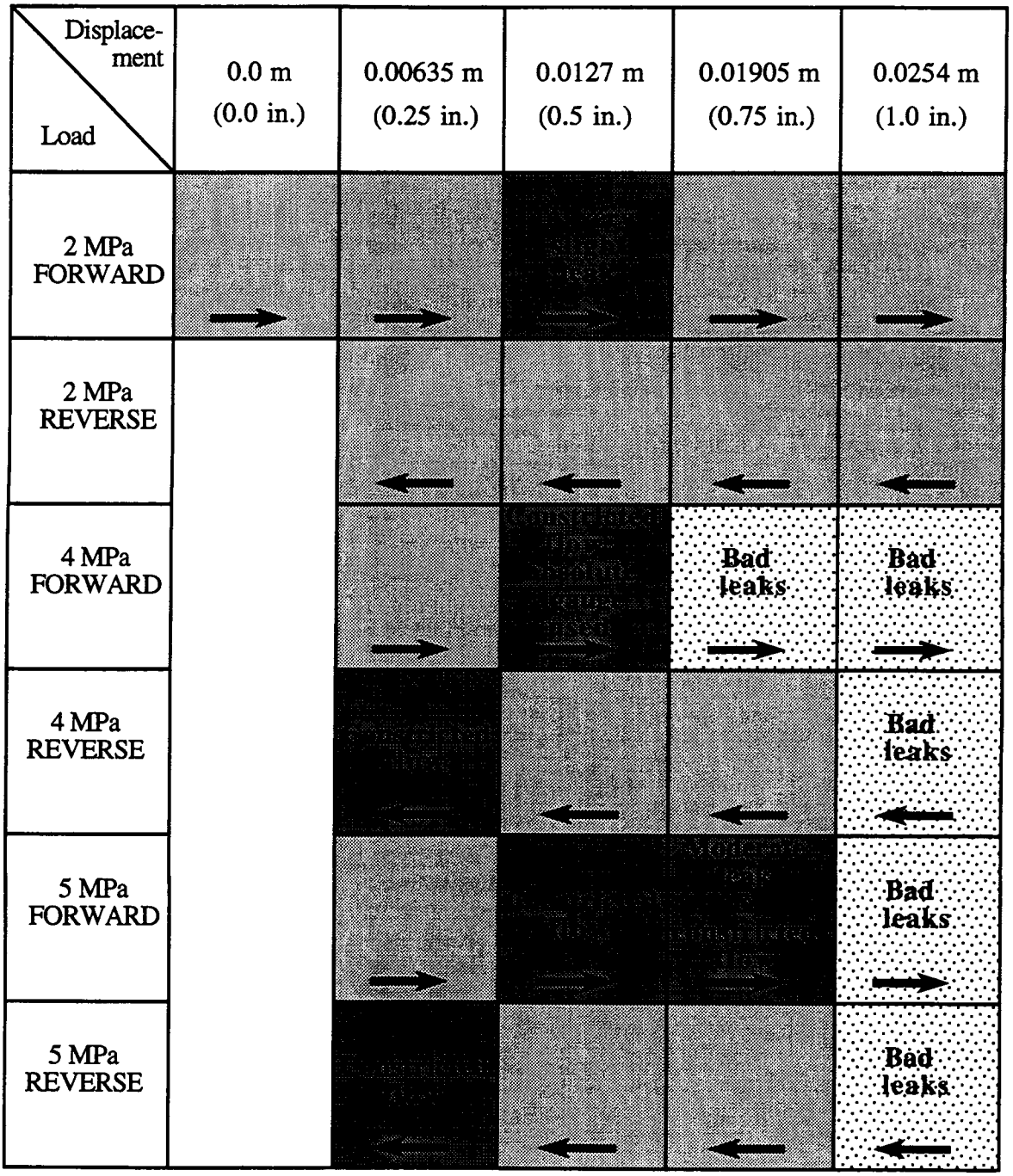

Figure 3-17. Chart showing the experimental difficulties during the shear displacement experiment

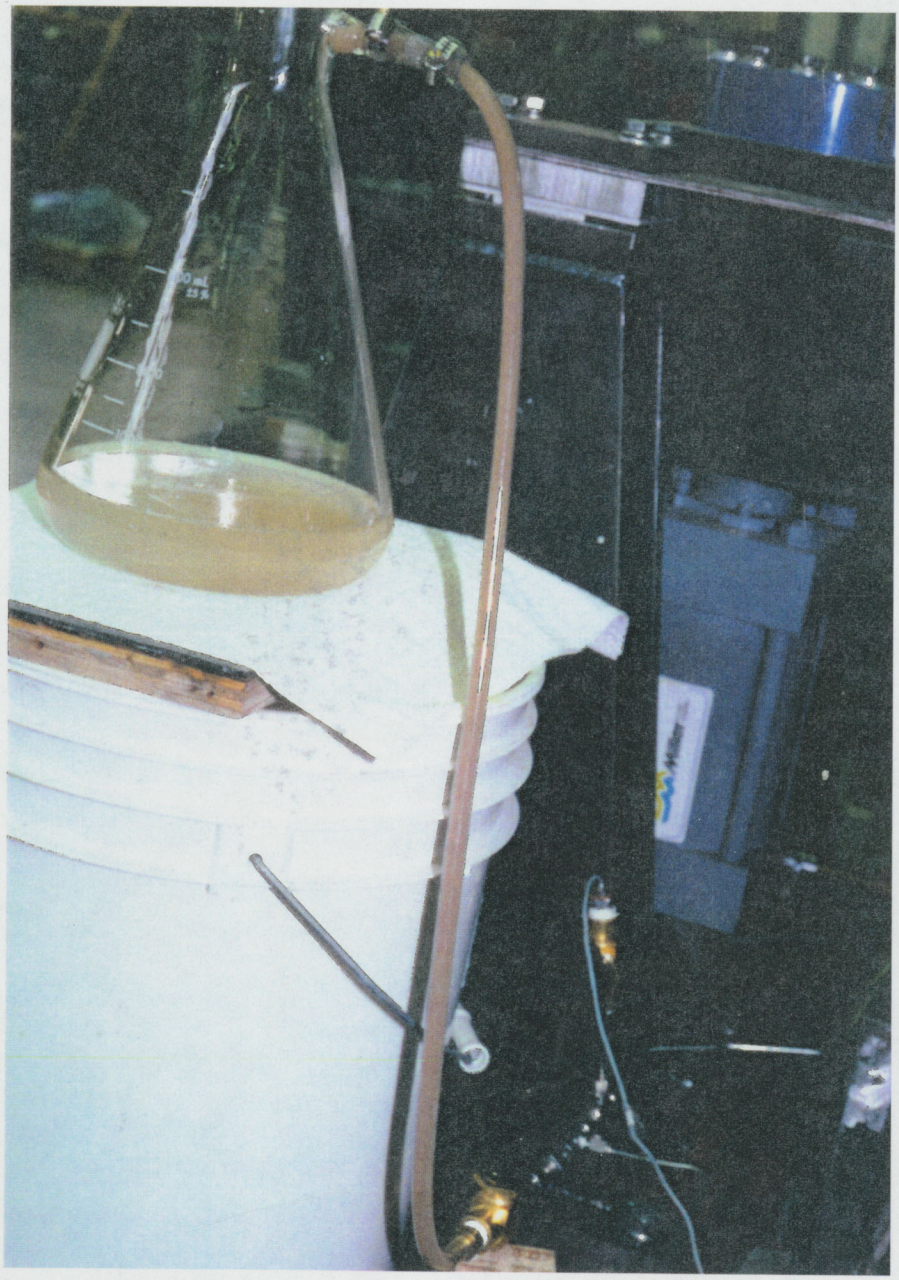

Figure 3-18. The fine particles suspended in effluent while flushing the system after displacement. This material was an early indication of the gouge formation.

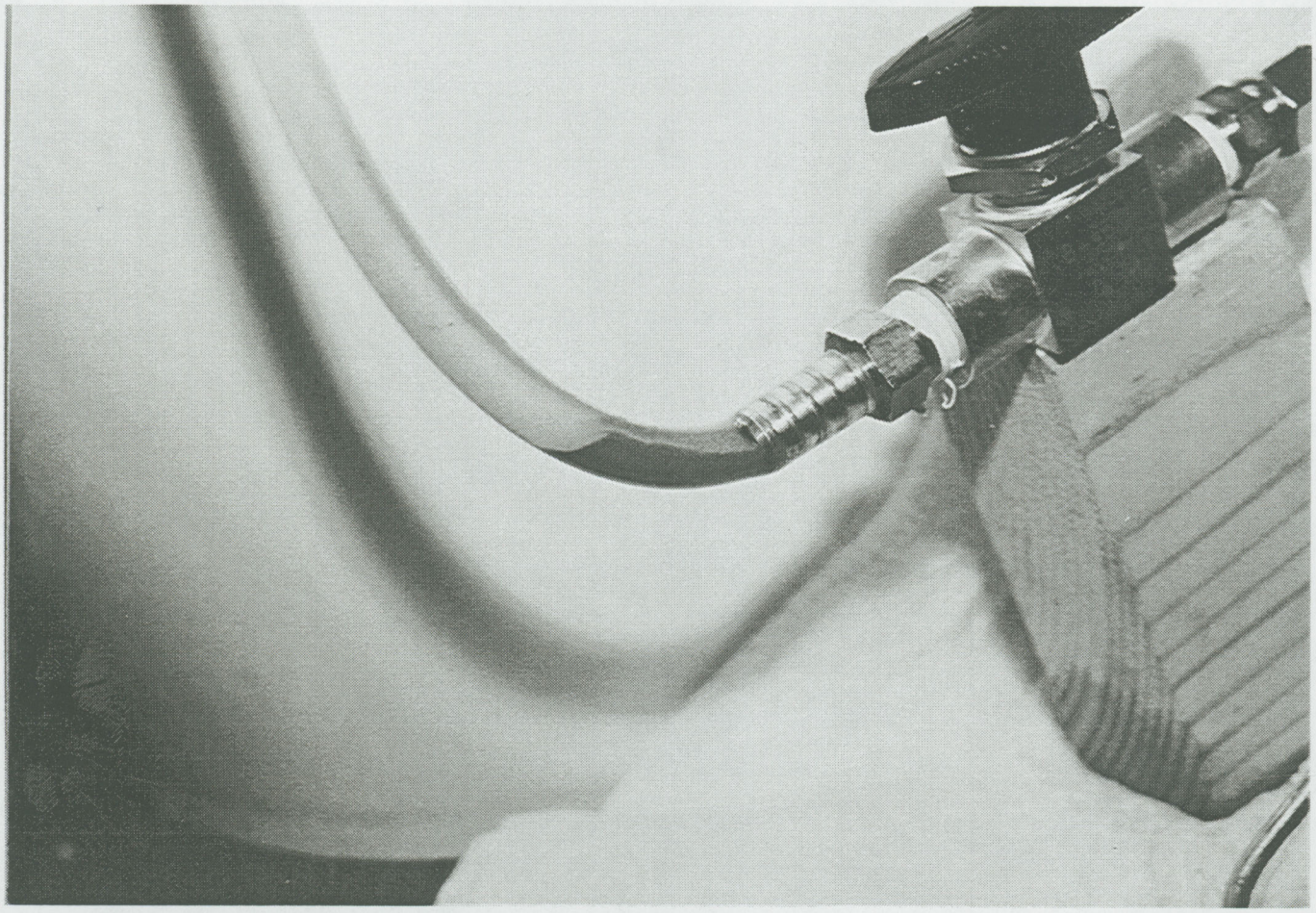

Figure 3-19. The fine particle accumulation due to settling. This material must be removed before data recording for steady-state flow.

Figure 3-20. Slow settling causes slug flow, which may influence steady-state experiment

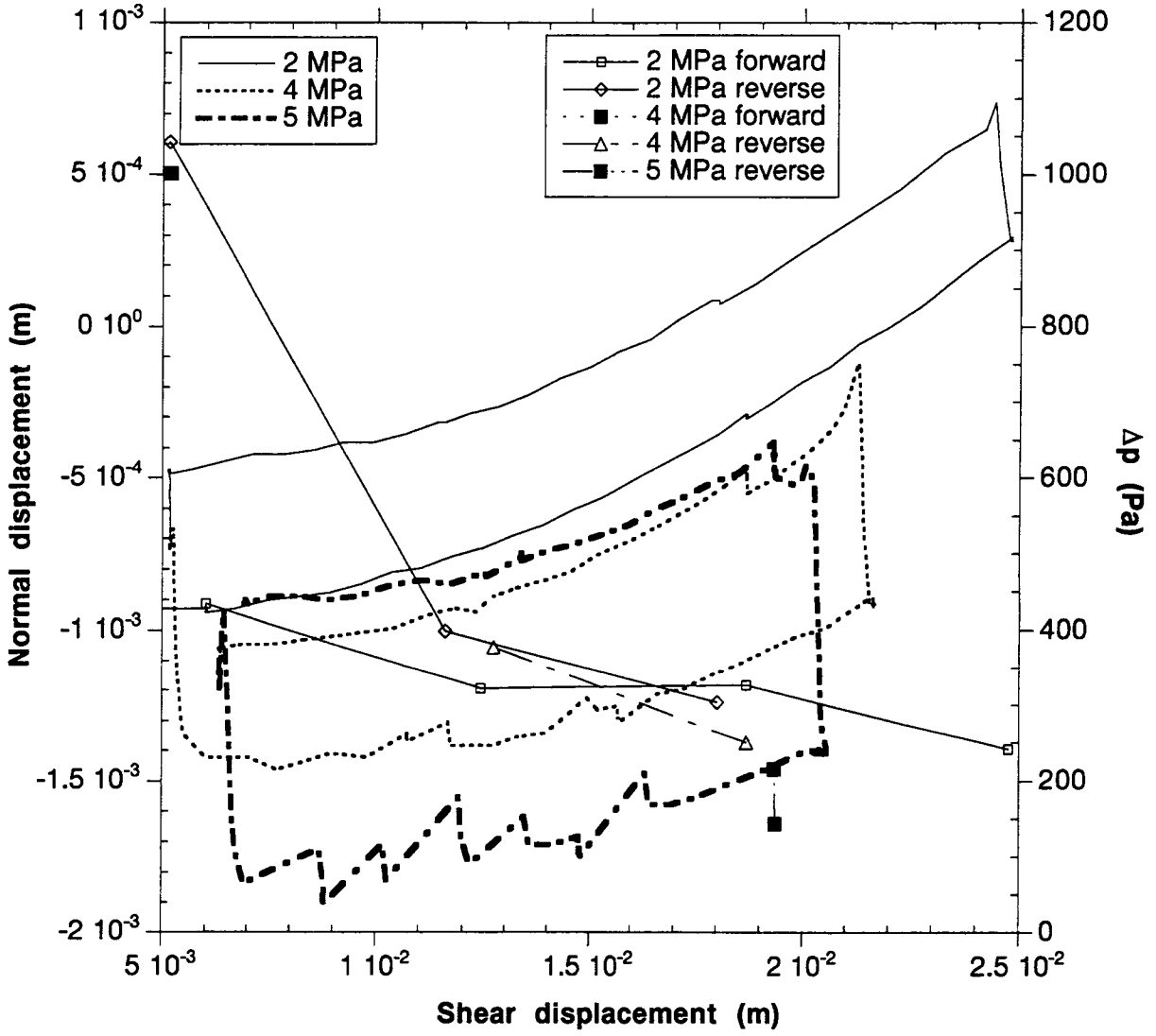

Figure 3-21. Superposition of pressure drop data on the plot between vertical displacement versus shear displacement

Figure 3-22. The paste-like gouge material formed during shear displacement

existed downstream, the injected fluid was allowed to flow at high rates during the shearing; no air was expected to enter into the rock joint during such leaks.

Massive fractures parallel to the shear displacement direction but orthogonal to the joint plane developed during the shear displacement experiments. The largest fracture developed in the bottom block, almost splitting the rock into two pieces. This condition is clearly seen in Figures 3-5 and 3-23. Fractures relatively smaller in size also developed in the upper block, though they are not clearly visible. These fractures were not visible even after 8 MPa normal stress being applied. Whether these new fractures grew from existing and hidden fractures could not be determined.

It should be noted that shear testing is a destructive method of testing. It is clearly evident that the damage of the rough surface produces a significant amount of fine particles. The texture of these fine particles can be seen in Figure 3-24. The amount of fine particles is significant, and it is necessary to separate the effect of dilation on the flow from the effect of fine particle on the flow. However, from the data acquired during the first displacement cycle under 2 MPa normal stress, before a significant amount of fine particles was formed, one could make qualitative statements on the effect of dilation. Maximum increase and decrease in the permeability of the fracture during 0.0254 m (1 in.) shear displacement was observed to be 40 and 20 percent, respectively.

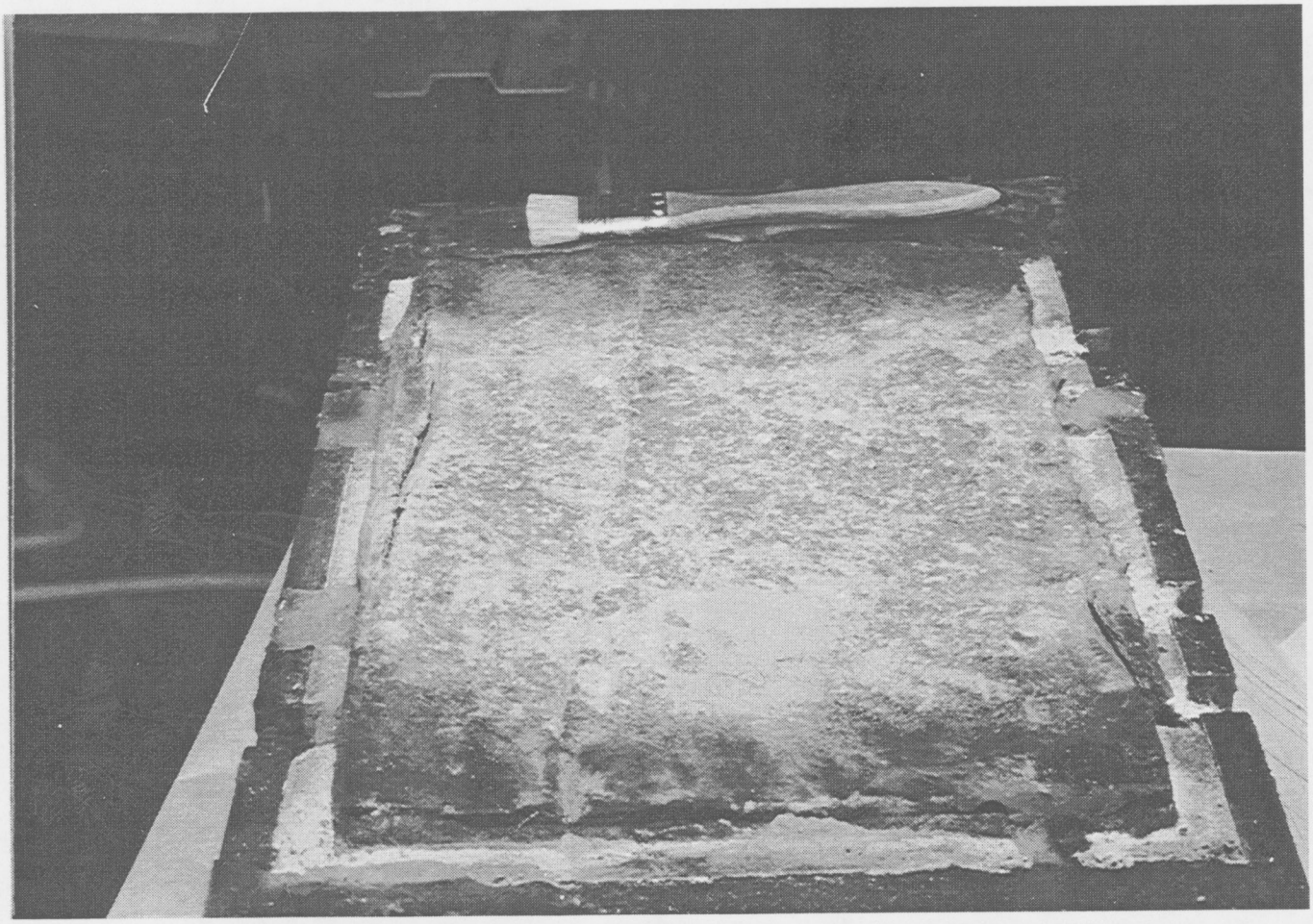

Figure 3-23. The massive fracture in the lower block developed during shear displacement

Figure 3-24. Gouge material after being dried to demonstrate texture and particle size

4 CONCLUSION

The change in rock-joint permeability under normal and shear loads has been investigated. Results from testing one specimen of Apache Leap Tuff have been analyzed and presented in this report. An increase in normal stress to 8 MPa caused nearly a 35 percent change in fracture permeability. Forward and reverse normal stress showed a definite hysteresis in the fracture permeability, with a similar trend being observed from the mechanical aperture measurements. As expected, the fracture permeability gave a nonlinear trend with the imposed normal stress.

Based on the data collected thus far, a permeability change of nearly 350 percent has been observed when the specimen was subjected to a combined production of gouge material and joint dilation due to shearing. However, from the limited tests conducted to date, it was not possible to separate the permeability change due to gouge material production from that due to dilation.

Former investigators had been able to test the effect of shear up to a maximum displacement of $6.35 \times 10\text{-}3$ m (0.25 in.). The apparatus developed has demonstrated a capability for measuring the effect of up to 0.0254 m (1 in.) of shear displacement on permeability, though theoretically, a displacement of up to 5.08×10^{-2} m (2 in.) can be studied. Based on the results from the test, it appears that the effect of shearing is much more significant than demonstrated in the past. However, it must be noted that the level of damage may be a function of surface characteristics in addition to the rock material properties. In this regard, this experiment used Apache Leap tuff whose characteristics are similar to the welded tuff that occurs at the repository horizon at YM. However, additional rocks with different material properties, and more Apache Leap specimens must be tested before the results can be considered conclusive.

Performing shear load experiments was much more difficult compared to the normal load experiments, due primarily to the extreme conditions under which the fluid-sealing mechanism is operated. This difficulty, in addition, is complicated by the fact that shear testing is a destructive method of testing. It is clearly evident that the damage of the rough surface produces a significant amount of fine particles. Thus, it is necessary to separate the effect of dilation from that of gouge material on the flow.

Numerical exercises were performed to retrieve aperture data from block surface height data. The FRAC_APR code was written that searched for the perfect mate between the two blocks. While the method seemed to have found the matching position, the quantitative aperture data do not seem reasonable. Further numerical studies are necessary.

5 FUTURE PLANS

5.1 EXPERIMENTAL DIFFICULTIES

The current experiment was interrupted by leaks, malfunctioning of the transducers for water-saturated experiments, breakdown of cylinder switching valve, and asynchronization of the piston movement with the driving motor. Difficulties were also experienced in the airflow measurements at both high and low flow rates. At low flow rates, the bubble flowmeter was affected by the interfacial tension at the glass wall whereas at high flow rates creation of multiple bubbles forced the experiment to be repeated several times.

Work is in progress to test the repeatability of the normal load experiment. Preparation is also under way to test the pressure drop at a steady flow rate under shear load conditions at various normal loads. The data presented in the figures are currently under analysis to extract saturated hydraulic conductivity and thus the effective joint aperture.

5.2 FUTURE MODIFICATION OF APPARATUS

Several modifications to the test apparatus are under consideration.

- In order to prevent the distortion of the box during the MH test under combined normal and shear loads, the design of the grout box, as well as the grouting process, will be modified.
- A wide neck particle arrester (trap) can be attached to the outlet end and outside of the grout box so that the surroundings of the outlet valves will not need frequent cleaning.
- A panel of differential pressure transducers will be used in order to measure the pressure drop during constricted flow conditions.

To be able to measure high-pressure drop as a result of the production of massive amounts of fine particles, the apparatus must be capable of withstanding the pressure exerted. Attempts will be made to measure pressure drops up to 690 kPa (100 psi). It should also be noted that, in the absence of gouge, the pressure drop across an 8-in. length of the fracture used in this experiment is less than 0.0508 m (2 in.) of water at 6.66×10^{-8} m^3/s (4 cm^3/min) flow rate. Such low-pressure drops can be affected by electrical noise, temperature change, and slight fluctuations in fluid pumping. Therefore, the shear experiment will pose difficulties at two extremes while measuring change in permeability.

5.3 MODELING-RELATED ISSUES

Since conducting experiments using more than a limited number of samples is prohibitively expensive, a mathematical/computer model is often developed to predict hydraulic conductivity properties from the joint surface properties and to develop or identify scaling parameters. An effort is under way to correlate the joint roughness to flow channeling and joint permeability. With this purpose in mind, the rock joint surfaces have been profiled by using laser profilometer. Since the top and bottom blocks are of different sizes, and profiling is done by separating the mated joint, appropriate matching of the two faces must be done in order to retrieve the aperture data. The aperture data retrieved so far have been deemed unacceptable even after the use of a numerical technique to obtain the best match. The

mathematical minima in the sum of the square differences in the surface heights resulted in aperture values of the order of 5 to 10 mm at some locations. The numerical matching exercise was conducted by moving the upper block on the lower block, which was held fixed. The movement was mostly translational, and there is evidence that rotational movement is necessary to obtain better matching. A better technique must be adapted so as to retrieve accurate aperture data.

Efforts will also be expended toward developing a mathematical/computer model to predict hydraulic conductivity properties from the normal load data, profilometry data, and dilation data. The model will be validated by using the injection rate and outflow rates from various channels obtained from the experiments described above. The model will also use data collected from the radial flow experiments to obtain a relationship between preferential paths and applied normal loads. The joint-face mismatching that is likely to take place during the sample mounting process will also be numerically corrected.

Other pertinent questions that arise regarding simulation studies include:

- Should the saturation versus unsaturated conductivity be directly used in the numerical simulation or should it be scaled up to the individual joint size that will be accounted for in the numerical simulator? Is a model available to go from the laboratory scale [i.e., 0.2032×0.2032 m (8 in. $\times$ 8 in.)] to grid scale (for example 20 m$\times$20 m)?

- What if the mathematical prediction does not match the experimental data? Should one further the study to understand the physics of the problem (such as flow regime, viscous-capillary force interplay, etc.)?

6 REFERENCES

Althaus, E., A. Friz-Topfer, C. Lempp, and O. Hatau. 1994. Effects of water on strength and failure mode of coarse-grained granites at 300 °C. *Rock Mechanics and Rock Engineering* 27: 1-21.

Amyx, J., D.M. Bass Jr., and R.L. Whiting. 1960. *Petroleum Reservoir Engineering Physical Properties*. New York, NY: McGraw-Hill Book Company.

Buscheck, T.A., and J.J. Nitao. 1993. The analysis of repository-driven hydrothermal flow at Yucca Mountain. *Proceedings of the Fourth International Conference on High Level Radioactive Waste Management*. La Grange Park, IL: American Nuclear Society.

Buscheck, T.A., and J.J. Nitao. 1994. The impact of buoyant, gas-phase flow and heterogeneity on thermo-hydrological behavior at Yucca Mountain. *Proceedings of the Fifth International Conference on High Level Radioactive Waste Management*. La Grange Park, IL: American Nuclear Society: 2,450-2,474.

de Marsily, G. 1987. An overview of coupled processes with emphasis on geohydrology. *Coupled Processes Associated with Nuclear Waste Repositories*. C.F. Tsang, ed. San Diego, CA: Academic Press: 27-37.

Ghosh, A., S.M. Hsiung, M.P. Ahola, and A.H. Chowdhury. 1993. *Evaluation of Coupled Computer Codes for Compliance Determination*. CNWRA 93-005. San Antonio, TX: Center for Nuclear Waste Regulatory Analyses.

Ghosh, A., S.M. Hsiung, G.I. Ofoegbu, and A.H. Chowdhury. 1994. *Evaluation of Computer Codes for Compliance Determination Phase II*. CNWRA 94-001. San Antonio, TX: Center for Nuclear Waste Regulatory Analyses.

Hill, D.P., et al. 1993. Seismicity remotely triggered by the magnitude 6.3 Landers, California, earthquake. *Science* 260: 1,617-1,623.

Hsiung, S.M., A.H. Chowdhury, W. Blake, M.P. Ahola, and A. Ghosh. 1992. *Field Site Investigation: Effect of Mine Seismicity on a Jointed Rock Mass*. CNWRA 92-012. San Antonio, TX: Center for Nuclear Waste Regulatory Analyses.

Hsiung, S.M., D.D. Kana, M.P. Ahola, A.H. Chowdhury, and A. Ghosh. 1994. *Laboratory Characterization of Rock Joints*. NUREG/CR-6178. Washington, DC: Nuclear Regulatory Commission.

Iwai, K. 1976. *Fundamental Studies of Fluid Flow Through a Single Fracture*. Ph.D. Thesis. Berkeley, CA: University of California at Berkeley.

Kana, D.D., B.H.G. Brady, B.W. Vanzant, and P.K. Nair. 1991. *Critical Assessment of Seismic and Geomechanics Literature Related to a High-Level Nuclear Waste Underground Repository*. NUREG/CR-5440. Washington, DC: Nuclear Regulatory Commission.

Klavetter, E.A., and R.R. Peters. 1986. *Estimation of Hydrologic Properties of an Unsaturated Fracture Rock Mass.* SAND84-2642. Albuquerque, NM: Sandia National Laboratories.

Kumar, S., R.W. Zimmerman, and G.S. Bodvarsson. 1989. *Permeability of fracture with cylindrical asperities.* Report LBL-27626. Berkeley, CA: Lawrence Berkeley Laboratory.

Lin, W.A., and W.D. Daily. 1989. Laboratory study of fracture healing in Topopah Spring tuff—implications for near field hydrology. *Nuclear Waste Isolation in Unsaturated Zone Focus '89 Proceedings.* La Grange Park, IL: American Nuclear Society: 443-449.

Ofoegbu, G.I., S.M. Hsiung, A.H. Chowdhury, and J. Philip. 1994. *Field Site Investigation: Effect of Mine Seismicity on Groundwater Hydrology.* CNWRA 94-017. San Antonio, TX: Center for Nuclear Waste Regulatory Analyses.

Rojstaczer, S., and S.Wolf. 1992. Permeability changes associated with large earthquakes: An example from Loma Prieta, California. *Geology* 20: 211-214.

Schlichting, H. 1968. *Boundary Layer Theory*, 6th ed. New York: McGraw Hill. McGraw-Hill Book Company, Inc., New York.

U.S. Department of Energy. 1988. *Site Characterization Plan: Yucca Mountain Site, Nevada Research and Development Area.* DOE/RW-0199. Washington, DC: U.S. Department of Energy.